Research Article

Developmental Dynamics
DOI 10.1002/dvdy.24358

lin28 proteins promote expression of 17~92 family miRNAs during amphibian development

Fiona Warrander, Laura Faas, Oleg Kovalevskiy, Daniel Peters, Mark Coles, Alfred A Antson, Paul Genever and Harry V Isaacs*

Department of Biology,
Area 11,
Department of Biology,
University of York,
York, YO10 5DD
United Kingdom

***Corresponding author**
Harry V. Isaacs
Tel: +44 (0) 1904 328696
Fax: +44 (0) 1904 328505

Email: harry.isaacs@york.ac.uk

Received: Jul 14, 2015; Revised: Sep 22, 2015; Accepted: Sep 24, 2015

Abstract

Background: Lin28 proteins are post-transcriptional regulators of gene expression with multiple roles in development and the regulation of pluripotency in stem cells. Much attention has focussed on Lin28 proteins as negative regulators of *let-7* miRNA biogenesis; a function that is conserved in several animal groups and in multiple processes. However, there is increasing evidence that Lin28 proteins have additional roles, distinct from regulation of *let-7* abundance. We have previously demonstrated that lin28 proteins have functions associated with the regulation of early cell lineage specification in *Xenopus* embryos, independent of a lin28/*let-7* regulatory axis. However, the nature of lin28 targets in *Xenopus* development remains obscure. **Results:** Here we show that mir-17~92 and mir-106~363 cluster miRNAs are down regulated in response to lin28 knockdown, and RNAs from these clusters are co-expressed with lin28 genes during germ layer specification. Mature miRNAs derived from *pre-mir-363* are most sensitive to lin28 inhibition. We demonstrate that lin28a binds to the terminal loop of *pre-mir-363* with an affinity similar to that of *let-7*, and that this high affinity interaction requires to conserved a GGAG motif. **Conclusion:** Our data suggest a novel function for amphibian lin28 proteins as positive regulators of mir-17~92 family miRNAs.

Keywords

lin28; mir-363; let-7; mir-17~92; mir-106~363; *Xenopus*,

Introduction

Lin28 proteins are post-transcriptional regulators

Lin28 family proteins are post-transcriptional regulators of development and adult homeostasis. They are RNA binding proteins, characterised by a unique combination of RNA binding cold shock and zinc knuckle domains. LIN-28 was initially identified as a regulator of developmental timing in *C.elegans* and is required for the self-renewal of stem cells, with mutations in LIN-28 leading to the precocious development of late cell lineages (Moss et al., 1997; Vadla et al., 2012). Mammalian embryonic stem cells also express high levels of Lin28 proteins, which, in combination with Nanog, Oct4 and Sox2, have been used to reprogram somatic cells to a pluripotent stem cell phenotype (Viswanathan and Daley, 2010). Lin28 family genes have also been implicated as regulators in a diverse range of other biological processes, including glucose homeostasis, tissue regeneration and the onset of puberty in both mice and humans (Shyh-Chang and Daley, 2013; Shyh-Chang et al., 2013).

Research in a number of different systems has focused on the conserved role of Lin28 proteins as negative regulators of *let-7* family miRNAs. Lin28 proteins interact with both primary and precursor *let-7* miRNAs to inhibit the biogenesis of the mature biologically active forms. A prevalent model indicates an inverse relationship between levels of Lin28 proteins and mature *let-7* miRNAs (Viswanathan, 2008; Viswanathan and Daley, 2010). Typically, reduction in Lin28 function leads to increased levels of mature *let-7* miRNAs. This regulatory interaction between Lin28 proteins and *let-7* miRNAs is clearly important in multiple contexts, however, there is also increasing evidence for interactions of Lin28 proteins with a wider range of RNA targets, including other miRNA families and multiple protein coding mRNAs (Mayr and Heinemann, 2013). In the latter situation, interaction with Lin28 proteins has been shown to affect the translation of the target mRNA (Mayr and Heinemann, 2013; Shyh-Chang and Daley, 2013).

Lin28 function in amphibian development

In an earlier study we identified *lin28a* as a transcriptional target of FGF signalling (Branney et al., 2009). Subsequently, we investigated the function of the two Lin28-related genes, *lin28a* and *lin28b*, in *Xenopus* (Faas et al., 2013). We showed that compound knockdown of lin28a and lin28b in early development disrupts the development of axial and paraxial mesoderm. Our data indicate that lin28 function is required in pluripotent

cells of the early *Xenopus* embryo for the normal response to mesoderm inducing growth factors signals, such as FGF and activin.

Identifying miRNA targets of amphibian lin28 proteins

At present, the nature of lin28 target RNAs in the early amphibian embryo remains elusive. Our data show that *Xenopus* lin28a and lin28b are able to interact with the terminal loop of *let-7* miRNAs (Faas et al., 2013). However, inhibition of lin28 function in *Xenopus* does not lead to significant increases in the levels of mature *let-7* miRNAs in the early embryo. Therefore, the earliest perturbations in amphibian development, resulting from lin28 knockdown, do not arise from effects on a lin28/*let-7* axis (Faas et al., 2013).

In the present study we have undertaken a microarray based analysis to determine if other miRNAs are regulated by lin28 in gastrula stage amphibian embryos. In contrast to the prevailing model, in which Lin28 proteins act as negative regulators of miRNA biogenesis, we find that lin28 knockdown leads to significant down-regulation of several miRNAs. Prominent amongst these are *mir-363-5p* and *mir-363-3p*, which are derived from a common *mir-363* precursor RNA.

mir-363 belongs to the mir-17~92 family of miRNAs, which are encoded by the mir-17~92, mir-106a~363 and mir-106b~25 genomic clusters. These paralogous clusters are transcribed to produce polycistronic RNAs, which are subsequently processed to form multiple, mature miRNAs with a range of related seed sequences and target specificities (Olive et al., 2010; Mogilyansky and Rigoutsos, 2013). Significantly, we find that several other miRNAs from both the mir-17~92 and mir-106a~363 clusters are also down-regulated in response to lin28 inhibition, indicating that *Xenopus* lin28 proteins may have a wider role in regulating the abundance mir-17~92 family miRNAs.

We demonstrate that zygotic transcription of the mir-17~92 and mir-106a~363 clusters is initiated in the *Xenopus* embryo during the period of germ layer specification. We show that *mir-363-5p* and *mir-363-3p* are both expressed in the early mesoderm and later in the neuroectoderm in domains overlapping with those previously reported for *lin28a* and *lin28b* (Faas et al., 2013), suggesting a possible role for a lin28/mir-17~92 regulatory axis in the process of germ layer specification.

The mechanism by which lin28 proteins regulate the abundance of mir-17~92 family miRNAs remains unclear, however, we show here that lin28a protein physically interacts with a GGAG motif in the in the terminal loop of the *pre-mir-363* miRNA. Our data support

a novel function for *Xenopus* lin28 proteins as positive regulators of *mir-363* miRNA abundance.

Results

Analysis of miRNA abundance in lin28 morphant embryos

We have previously reported the efficient knockdown of endogenous *Xenopus* lin28 proteins using a combination of antisense morpholino oligos (AMOs) directed against the three lin28 isoforms (lin28a1, lin28a2 and lin28b) expressed in the embryo. In contrast to the predictions of the prevailing model for Lin28 function, we found no evidence for change in *let-7* abundance at gastrula stages following lin28 knockdown (Faas et al., 2013). This begs the question, are there other miRNA targets of lin28 proteins in the earliest stages of amphibian development? In order to begin to address this question, we have used the same AMOs to efficiently knockdown endogenous lin28 proteins (Figure 1A) and microarray analyses to identify changes in the abundance of miRNAs in lin28 knockdown embryos (lin28 morphants) at two different stages (early gastrula stage 10.5 and late gastrula stage 13). These screens were carried out using the Affymetrix microarray platform at stage 10.5 and the Exiqon microarray platform at stage 13 (Supplementary Tables 1 and 2).

An analysis of fold changes relative to controls of *Xenopus* miRNAs with an expression level of threshold >10 in control and lin28 morphant embryos at early gastrula stage 10.5 reveals a number of miRNAs changing in abundance. However, using a strict cut-off of ≥2 fold change and p ≤0.05, we find that only one miRNA (*mir-363-5p*) is significantly affected in lin28 morphants, in this case showing a 2.6 fold decrease, (p=0.049), indicating a positive role for lin28 in regulating the abundance of this miRNA.

At gastrula stage 13 more miRNAs are affected in Lin28 morphants. Table 1 shows the fold changes of *Xenopus* miRNA abundance in lin28 morphants relative to control embryos at stage 13. Only miRNAs flagged as being detected in all replicate arrays were included in this table. We find that several miRNAs show significant (≥2 fold change and p≤0.05) changes in abundance in stage 13 lin28 morphants, including *mir-363-3p,* which, like *mir-363-5p*, is processed from a common *mir-363* precursor RNA. The *mir-363* precursor is derived from a polycistronic primary RNA which is transcribed from the mir-106a~363 locus of clustered miRNAs; a paralogue of the well characterised mir-17~92 miRNA cluster. Figure 1B shows the organisation of the *X.tropicalis* mir-17~92 and mir-16~363 loci as derived from the *X.tropicalis* genome sequence. As indicated in Table 1, 6/8 of the

significantly changing miRNAs are transcribed from these clusters, with the abundance of all decreasing in lin28 morphants.

We next investigated quantitative changes in the levels of a number of mir-17~19 and mir-106a~363 cluster miRNAs in lin28 morphants by qRT-PCR. Again we see significant decreases in the abundance of several 17~92 family miRNAs (Figure 1C), including *mir-363-3p* and *mir-363-5p*. There is good evidence that GGAG or closely related motifs in the terminal loop regions of pre-miRNAs are important for recognition and binding by the zinc knuckle domain of lin28 proteins (Mayr and Heinemann, 2013). Here we show that such a GGAG is present in the *Xenopus mir-363* precursor RNA. Figure 1D indicates the putative lin28 binding motif and highlights the predicted sequences of the mature *mir-363-5p* and *mir-363-3p* miRNAs.

Analysis of miRNA abundance in lin28 over-expressing embryos

We were interested to see how over-expression of the three *Xenopus* lin28 proteins affected embryo development and the abundance of 17~92 family miRNAs. Figure 2A is a Western blot showing levels of each protein in embryos injected with 1ng of each of the synthetic lin28 mRNAs. In contrast to the Western blot in Figure 1A, the exposure presented does not detect endogenous lin28 proteins in control uninjected embryos, indicating that mRNA injection leads to massive overexpression of each of the lin28 proteins relative to normal endogenous levels. Interestingly, overexpression of lin28 proteins does not result in gross developmental abnormalities (Figure 2B) or significant changes in the abundance of mature mir-17~19 and mir-106a~363 cluster miRNAs (Figure 2C).

Physical interaction of recombinant lin28a protein with the mir-363 terminal loop

As with lin28 regulation of *let-7* miRNAs, it is possible that lin28 regulation of *mir-363* abundance involves a physical interaction of the protein with the miRNA terminal loop. We used RNA electromobility shift assays (EMSAs) to investigate whether *Xenopus* lin28 proteins bind to *pre-mir-363* RNA. We purified a recombinant, truncated version of the *X. tropicalis* lin28a (Xrt-lin28a). This protein construct of residues 34-177, contains both the cold shock and zinc-knuckle RNA binding domains, but lacks segments of N-terminal and C- terminal residues, which were predicted to be disordered (Figure 3A). In order to determine if terminal truncations affect binding to canonical RNA targets, we compared the abilities of recombinant, full-length human and N- and C- terminally truncated human LIN28A (rt-LIN28A, residues 37-180) to bind the terminal loop of a *let-7-g* precursor RNA;

a well characterised lin28 target, which we have previously shown to be bound by *in vivo* translated *Xenopus* lin28 proteins (Faas et al., 2013). Figure 3B shows that full length and truncated human LIN28A proteins have a similar ability to bind *let-7g* RNA. In keeping with these observations, we find that that Xrt-lin28a is also able to bind the *let-7g* terminal loop with high affinity (K_d= 314 nM) (Figure 3C). We provide additional evidence that Xrt-lin28a maintains its ability to discriminate genuine target RNAs. *Pre-mir-138* has previously been shown to be ineffective at competing with pre-let-7 for binding of Lin28a protein, indicating that the terminal loop of *mir-138* is not a high affinity target of Lin28 proteins (Piskounova et al., 2008). Figure 3D shows that Xrt-lin28a protein also exhibits little binding activity towards the terminal loop of *mir-138* (L-mir-138). Even at the highest protein concentrations tested, the proportion of radiolabelled L-mir-138 bound is only 22%.

Figure 4A shows that Xrt-lin28a binds to the terminal loop region of *pre-mir-363* (L-mir-363) with a similar affinity (K_d= 448 nM) to its binding with the *let-7g* terminal loop. Further evidence for the specific nature of this interaction is demonstrated by the observation that excess cold L-mir-363 competes more efficiently for binding of radiolabelled L-mir-363 to Xrt-lin28a, than does the non-relevant L-mir-138 RNA. Thus, in the presence of a 100-fold excess of cold L-mir-363 only 3% radiolabelled L-mir-363 remains bound to Xrt-lin28a, whereas 27% remains bound in the presence of 100-fold excess of L-mir-138 RNA (Figure 4B).

We next investigated the importance to L-mir-363 binding of the GGAG sequence motif present in the mir-363 terminal loop. A mutant *mir-363* terminal loop RNA (mL-mir-363), in which the GGAG sequence was replaced by a GUAU, was synthesised. The same substitutions have previously been shown to reduce the ability of Lin28 to bind to *let-7* (Heo et al., 2009). Figure 4C shows that Xrt-lin28a has a reduced ability to bind mL-mir-363 compared to the GGAG containing L-mir-363 RNA. Binding of radiolabelled L-mir-363 in the presence of 12.8 µM Xrt-lin28a protein approaches 100%, whereas the binding of the mutant mL-mir-363 RNA is reduced to 58%.

Physical interaction of endogenously translated lin28a isoforms with pre-mir-363

Our experiments using truncated recombinant *Xenopus* lin28a protein have allowed us to investigate the properties and specificity of interactions with the *mir-363* terminal loop sequence. However, it is important to note that alternative splicing of small 5' protein coding exons gives rise to two lin28a protein isoforms (lin28a1 and lin28a2) in *Xenopus* (Faas et al., 2013). To investigate binding of these two isoforms to *mir-363* we have made use of the ability to overexpress specific proteins from injected synthetic messenger RNAs

in the cells of *Xenopus* embryos. Extracts from embryos overexpressing individual isoforms can then be used as a source of full-length, *in vivo* translated proteins for use in EMSA assays. Figure 5A and 5B show that extracts from embryos overexpressing either lin28a1 or lin28a2, but not control, non-overexpressing embryos, contain L-mir-363 binding activity. Moreover, we can attribute this binding activity to the overexpressed lin28a proteins because we are able to use an anti-lin28a antibody, but not a pre-immune serum, to deplete the band corresponding to the L-mir-363+lin28 complex, giving rise to a higher molecular weight supershifted L-mir-363+lin28+Ab complex.

In order to recapitulate more accurately the binding of the full-length lin28a isoforms to the native *pre-mir-363* structure we carried out similar binding studies with an *in vitro* transcribed RNA corresponding to the putative full length *pre-mir-363*. Again we see that extracts from lin28a overexpressing embryos contain a *pre-mir-363* binding activity which can be depleted with a lin28a antibody (Figure 5C and 5D). Interestingly, all embryo extracts contain at least two additional *pre-mir-363* binding activities (asterisks) distinct from that provided by the overexpressed lin28a proteins.

Temporal and spatial expression of mir-17~92 and mir-106a~363 clusters in the embryo.

We have provided evidence for a novel lin28 regulated pathway, involving mir-17~92 family miRNAs. However, for the proposed regulatory interactions to be relevant to normal development the components must be expressed in the same cells of the early embryo. We therefore investigated the temporal expression of the primary transcripts from the mir-17~92 cluster and mir-106a~363 clusters. Primary transcripts for both the mir-17~92 and mir-106a~363 clusters are initially detected by semi-quantitative rt-PCR at mid-blastula stage 8 (Figure 6A). This corresponds to the time when the zygotic expression of *lin28a* is initiated (Faas et al., 2013). Figure 6B shows embryos hybridised with RNA probes designed to detect the primary transcripts from the mir-17~92 and mir-106a~363 clusters in the developing embryo. Highest levels of expression are detected in the dorsal marginal zone of the embryo at early gastrula stage 10.5.

Spatial expression of mir-363-3p and mir-363-5p in the embryo.

Our data provide the strongest evidence for a direct regulatory interaction between amphibian lin28 proteins and the mir-17~92 family member, *mir-363*. Anti-sense locked nucleic acid (LNA) probes contain modified nucleotides, providing increased sensitivity in detection short RNA sequences, such as miRNAs, and have previously been used to

obtain highly specific *in situ* miRNA localisation in *Xenopus* (Sweetman et al., 2006). Figure 6C and 6D are *in situ* hybridisation analyses with antisense LNA probes specific for *mir-363-3p* and *mir-363-5p*. As with the primary cluster transcripts, highest levels of expression are detected in the dorsal marginal zone at the start of gastrulation. Later in development *mir-363* miRNAs are enriched in the dorsal neural plate. Both miRNAs exhibit expression patterns similar to those previously reported for *lin28*a and *lin28b* (Faas et al., 2013).

Discussion

let-7 levels are unaffected in gastrula stage lin28 morphants

We have previously shown that lin28 function is required for the very earliest responses of pluripotent cells in the amphibian embryo to germ layer specifying growth factors. For example, levels of mesoderm lineage specific marker genes such as *brachyury*, *myoD* and *chordin* are significantly reduced in early gastrula stage compound lin28 morphants (Faas et al., 2013). Furthermore, we found that levels of mature *let-7a, f* and *g* miRNAs are not significantly affected in gastrula stage lin28 morphants, leading to the proposition that, during the very earliest stages of amphibian development, lin28 proteins have functions independent of regulating *let-7* biogenesis. Here we complement and extend this analysis using miRNA microarray-based assays, and again we detect no significant changes in the levels of any of the *let-7* family miRNAs represented on either microarray platform (*let7a, b, c, e, f, g* and *i*) in gastrula stage lin28 morphants. However, we note that expression levels of *let-7* miRNAs are generally low and some family members are not detected at all (data not shown). Similar conclusions were drawn in a zebrafish lin-28 knockdown study, where no significant changes in *let-7* expression were found in morphants at 5 hpf (Ouchi et al., 2014). Interestingly, in *Xenopus* and zebrafish, increased levels of *let-7* miRNAs are detected in lin28 morphants during later development, post-neurula stage 22 and 28 hpf, respectively, indicating that in both species there is an early *let-7* independent, and a late *let-7* dependent role for lin28 proteins (Faas et al., 2013; Ouchi et al., 2014).

17~92 and 106~363 cluster miRNAs are down regulated in gastrula stage lin28 morphants

Our array analysis of morphants indicates no significant up regulation of any miRNAs. However, a number of miRNAs are shown to be down regulated, indicating a novel role for *Xenopus* lin28 proteins as positive regulators of miRNA abundance. A notable feature of this down regulated group is the enrichment for members of the mir-17~92 cluster (*mir-17-*

5p, *mir-19a* and *mir-20a*) and the paralogous mir-106~363 cluster (*mir-19b*, *mir-20b*, *mir-363-5p* and *mir-363-3p*). These data suggest a novel regulatory interaction, where lin28 proteins act as positive regulators of 17~92 family miRNAs.

Interestingly, we find that increasing levels of lin28 proteins does not lead to a significant complementary up regulation of 17~92 family miRNA abundance. This suggests that endogenous levels of lin28 proteins are sufficient to allow maximal production of mature 17~92 family miRNAs. Thus, lin28 levels only become limiting following knockdown. This is supported by the observations that lin28 morphants exhibit a strong phenotype, which can be rescued by lin28 mRNA injection (Faas et al., 2013), whereas embryos injected with lin28 mRNA alone develop normally (Figure 2B).

The paralogous mir-17~92 and mir-106~363 clusters each code for six miRNAs, which have been highly conserved during vertebrate evolution. The mir-17~92 cluster, in particular, has attracted a great deal of interest in recent years in relation to normal cellular function and its oncogenic potential (reviewed, (Mendell, 2008; Olive et al., 2010; Mogilyansky and Rigoutsos, 2013)). Studies in mammals indicate that 17~92 cluster miRNA expression is high in embryonic cells, and is associated with the pluripotent state. 17~92 miRNA expression has been proposed to be part of the miRNA signature of human embryonic and induced pluripotent stem cells (Wilson et al., 2009). Mutations in the 17~92 cluster are associated with Feingold syndrome in humans, which is characterised by skeletal dysplasia (Marcelis et al., 2008). Deletion of the 17~92 locus in mice also leads to abnormal skeletal development. The phenotype of 17~92 null mice indicates additional roles in embryonic growth and morphogenesis of the heart and lungs (Ventura et al., 2008; de Pontual et al., 2011).

The mir-106~363 cluster is less well studied. It has been reported that in mammals miRNAs from this cluster are not widely expressed and development of mice lacking the mir-106~363 cluster is apparently normal (Ventura et al., 2008). In contrast, we find that all six 106~363 cluster miRNAs are expressed by the early amphibian embryo (Supplementary Table 1). Of particular interest to the present study are *mir-363-5p* and *mir-363-3p*, which are derived from a common *mir-363* precursor RNA. Quantitative analysis of miRNA abundance in morphants indicate that, of the miRNAs analysed, *mir-363-5p* and *mir-363-3p* are most sensitive to lin28 inhibition.

Lin28 proteins bind the terminal loop region of multiple miRNAs

Lin28 proteins physically interact with primary and precursor *let-7* miRNAs (reviewed, (Mayr and Heinemann, 2013). This interaction is, in part, at least, mediated by GGAG or GGAG-related sequences in the terminal loop of *pre-let-7* miRNAs, and binding provides the basis for the negative regulatory effects of lin28 on the biogenesis of mature *let-7* miRNAs (Heo et al., 2009; Mayr and Heinemann, 2013). It is tempting to speculate that the physical interaction of lin28 proteins with 17~92 family RNAs might also be required for the positive regulatory interaction that we report here. It has been previously reported that LIN28A is able to bind to the human mir-363 precursor via a GGAG motif in its terminal loop (Heo et al., 2009). This GGAG motif is conserved in *Xenopus pre-mir-363* and both recombinant and endogenously overexpressed lin28a physically interact with the terminal loop sequence of *Xenopus pre-mir-363*. The affinity of this interaction is comparable with the observed for the interaction between lin28a and the *let-7g* terminal loop. Furthermore, we find that mutation of GGAG sequence in the *mir-363* terminal loop reduces the affinity of this interaction. In keeping with the notion that lin28 proteins and mir-17~92 miRNAs physically interact, we find that both *mir-363* miRNAs are expressed in similar domains to *lin28a* and *lin28b* in the presumptive mesoderm of gastrula stage *Xenopus* embryos (Faas et al., 2013).

Lin28 proteins inhibit the biogenesis of *let-7* miRNAs using multiple mechanisms. One reported mechanism requires LIN28A dependent recruitment of the Tut4 enzyme to a *pre-let-7* containing complex and subsequent Tut4 mediated polyuridylation and inactivation of *pre-let7* miRNAs (Heo et al., 2008; Heo et al., 2009). Several other human miRNAs have been shown to contain a terminal loop GGAG motif and are bound by LIN28A, however, this association does not always lead to Tut4 mediated polyuridylation and destabilisation (Heo et al., 2009). Thus, Lin28 binding to a GGAG motif in the terminal loop can have different consequences, depending on the target miRNAs involved.

At present, we do not know the mechanism by which amphibian lin28 proteins promote the expression of 17~92 family miRNAs in the early embryo. Indeed, our data do not rule out the possibility of lin28 proteins, indirectly or directly, regulating 17~92 miRNA expression by multiple mechanisms. However, an attractive hypothesis is that the binding of lin28 to the terminal loop region of the *pre-mir-363* sequence within the 106~363 polycistron somehow promotes subsequent processing to the precursor and mature miRNAs derived from the primary transcript. In regard to the related 17~92 polycistron, we have not yet investigated physical interactions with lin28 proteins. We have not identified GGAG-like

sequences in the terminal loop region of 17~92 polycistron derived pre-miRNAs, however, there are multiple GGAG motifs present within the intergenic regions of the polycistronic primary transcript (data not shown). It will be interesting to determine whether these motifs can act as binding sites for lin28 proteins.

Lin28, let-7 family and 17~92 family; key components of a pluripotency network

Lin28 expression is associated with pluripotent mammalian stem cells in culture and pluripotent cells in the early amphibian embryo that respond to the earliest lineage specifying growth factor signals. A key function of Lin28 proteins in mammalian stem cells is to inhibit the biogenesis of *let-7* miRNAs. During differentiation of stem cells lin28 levels fall and levels of biologically active *let-7* miRNAs rise (Viswanathan et al., 2008; Viswanathan and Daley, 2010). While a role for lin28 regulating *let-7* biogenesis in post-neurula stage amphibian embryos is supported, there is no evidence that this function is important in very early development, perhaps because transcription of *let-7* miRNAs is low. In contrast to *let-7* miRNAs, elevated expression of 17~92 family miRNAs is associated with the pluripotent state. It is tempting to speculate that in some pluripotent cell populations lin28 proteins might play a dual role in inhibiting *let-7* and promoting 17~92 family expression. We note that similar dual, opposite effects on the regulation of *let-7* and 17~92 miRNAs have also been reported for the hnRNPA1 RNA binding protein, which like Lin28 inhibits *let-7* biogenesis, but promotes the biogenesis of the 17~92 cluster miRNA, *mir-18a* (Guil and Caceres, 2007; Michlewski and Caceres, 2010).

Taken together, our results suggest a novel regulatory function for lin28 proteins in the pluripotent cells of the early amphibian embryo, in which lin28 proteins positively regulate levels of mature 17~92/106~363 cluster miRNAs in the early embryo, which contrasts with their activity of negatively regulating mature *let-7* miRNA levels in mammalian stem cell populations.

Experimental Procedures

Embryo methods

Xenopus tropicalis embryos were produced as previously described (Khokha et al., 2005; Winterbottom et al., 2010). Embryos were injected at 2- or 4-cell stage and cultured at 22ºC.

Samples for miRNA analysis were isolated using the miRVana miRNA isolation kit (Applied Biosystems). The protocol was carried out according to manufacturer's

instructions with the modification that after lysis samples were centrifuged for 10 minutes at 4°C and supernatant removed to a fresh tube.

Western bot analysis

Western blots were carried out as previously described, using affinity-purified *X. tropicalis* anti-lin28 antisera raised by inoculation of peptides corresponding to the C-terminal sequences of *X. tropicalis* lin28a1/a2 (EEQPISEEQELIPETME) or lin28b (SRKGPSVQKRKKT) proteins (Faas et al., 2013).

Knockdown of lin28a and lin28b

Compound knockdown of lin28a1+a2+b was accomplished using a total of 25ng per embryo of a mixture containing 10ng lin28a1+10ng lin28a2 + 5ng lin28b AMOs (Gene Tools, LLC), as previously described (Faas et al., 2013). Injections were carried out into all cells at either the two- or four-cell stage, with a maximum of 10 nl/embryo. Injections were targeted to the marginal zone.

Overexpression of lin28a and lin28b

The coding regions of *lin28a1*, *lin28a2* and *lin28b* were PCR amplified and sub-cloned into the Cs2+ mRNA transcription vector. mRNA synthesis was as previously described (Branney et al., 2009). All cells were injected at the two- or four-cell stage, with a total of 1 ng/embryo of each mRNA. Injections were targeted to the marginal zone.

Affymetrix miRNA array analysis

RNA was isolated from control embryos and knockdown as described above at early gastrula stage 10.5. The quality of the RNA was verified using the Agilent 2011 Bioanalyzer (Agilent). Samples were processed in the University of York, Department of Biology Technology Facility. 1µg samples were processed in the University of York, Department of Biology Technology Facility. RNA was labelled using HSR FlashTag Biotin RNA labelling kit (Genisphere) according to manufacturer's instructions, which included the addition of spike-in RNA controls to act as a method control. Samples were then hybridised to Genechips miRNA 2.0 (Affymetrix) overnight, and washed on a Fluidics Station 450 (Affymetrix), all carried out according to manufacturer's instructions. Scanning of the chips was carried out using an Affymetrix Genechip Scanner. CEL files were processed using Affymetrix QC tools software to provide background detection and quantile normalisation with a final median polish and log transformation. *Xenopus* feature data were extracted and statistical comparisons undertaken using a paired, 2-tail Student's t-test. The complete triplicate summarization data set for the *Xenopus* features are shown

in Supplementary Table 1. These data have been deposited in the ArrayExpress Archive (https://www.ebi.ac.uk/arrayexpress/) with accession number E-MTAB-3936.

Exiqon miRNA array analysis

Compound knockdown of lin28a1+a2+b was carried out as described above. Control embryos were injected with 30ng of a standard control MO. RNA was isolated from experimental embryos at late gastrula stage 13. Quality control, sample processing and preliminary data processing, including normalization were undertaken as a service by Exiqon A.S. Expression levels were calculated as fold changes relative to a mixed stage reference RNA sample. *Xenopus* feature data were extracted and statistical comparisons were undertaken using a paired, 2-tail Student's t-test. The median log ratios for the triplicate *Xenopus* data set are shown in Supplementary Table 2. These data have been deposited in the ArrayExpress Archive (https://www.ebi.ac.uk/arrayexpress/) with accession number E-MTAB-3939.

Semi-quantitative PCR analysis of miRNA cluster primary transcript abundance

Total RNA was extracted using TRI reagent (Sigma) according to the manufacturer's instructions. An additional precipitation step was undertaken using 7.5 M LiCl and 0.05 M EDTA at -80°C overnight. cDNA was synthesised from total RNA using 1 µg RNA random hexamers (Invitrogen) and SuperScript II Reverse Transcriptase (Invitrogen) according to manufacturer's instructions. cDNA was diluted 1/5 for use in RT-PCR reactions using PCR Master Mix (Promega). Primer sequences are shown below.

L8 forward:	GGGCTRTCGACTTYGCTGAA
L8 reverse:	ATACGACCACCWCCAGCAAC
miR-17~92 cluster forward:	TGCAGTGAAGGCACTTGTAG
miR-17~92 cluster reverse:	TAAACAGGCCGGGACAAG
mir-106a~363 cluster forward:	TGCTGGACACCTGTACT
mir-106a~363 cluster reverse:	TTCTGCGGTTTACAGATGGA

miRNA real-time quantitative PCR (qRT-PCR)

Samples to be used for miRNA analysis were isolated using the miRVana miRNA isolation kit (Applied Biosystems) as described above.

cDNA was synthesised from 10ng RNA/RT reaction with miRNA-specific primers for TaqMan assays (Applied Biosystems) using the TaqMan MicroRNA Reverse Transcription Kit (Applied Biosystems) as manufacturer's instructions.

qRT-PCR was carried out using TaqMan Universal Master Mix II (Applied Biosystems) with Taqman miRNA probes (Applied Biosystems) according to manufacturer's instructions. All reactions were performed in quadruplicate per sample on an ABI Prism 7000 detection system (Applied Biosystems) with thermal cycling at 95°C for 10 minutes, followed by 40 cycles of 95°C for 15 seconds and 60°C for 1 minute. Gene expression levels were normalised to U6 snRNA using the $2^{-\Delta\Delta Ct}$ method. Preliminary experiments had shown that U6 snRNA was a suitable control for this purpose (data not shown). Assays used were: hsa-miR-19b, hsa-miR-20b, hsa-miR-363#, hsa-miR-363, hsa-miR-18b, hsa-let-7a, hsa-let-7f, custom xtr-mir-106a (Applied Biosystems). It is important to note that the inclusion of stem loop structures in the primers used in the miRNA specific cDNA syntheses allow for the detection of mature, biologically active miRNAs.

Whole-mount in situ hybridisation for miRNA cluster primary transcripts

To generate whole-mount *in situ* hybridisation probes for the miR-17~92 and mir-106a~363 clusters cDNAs corresponding to sections of the miR-17~92 and mir-106a~363 primary transcripts were cloned in the pGEM®-T Easy vector following PCR amplification using *X.tropicalis* genomic DNA as template and the following primers.

mir-17~92 cluster forward: TGCAGTGAAGGCACTTGTAG

mir-17~92 cluster reverse: TAAACAGGCCGGGACAAG

mir-106a~363 cluster forward: TGCTGGACACCTGTACT

mir-106a~363 cluster forward: TTCTGCGGTTTACAGATGGA

DIG-labelled antisense *in situ* probes were transcribed and *in situ* hybridisation was carried out as previously described (Harland, 1991) with slight modification (Reece-Hoyes et al., 2002).

Whole-mount in situ hybridisation for miRNA

Probes used were 5'-DIG labelled locked nucleic acid (LNA) miRNA detection probes (Exiqon), named 'hsa-miR-363-3p', and 'xtr-miR-363*'. Protocol was carried out as described previously described previously (Sweetman, 2011), with modifications advised by Grant Wheeler,University of East Anglia,UK, personal communication). Probes were pre-absorbed six times by hybridising with the probe overnight against stage 35 embryos.

Colour development was with NBT/BCIP substrate. When signal began to develop, embryos were washed at 4°C overnight and subjected to repeat cycles of colour reaction and washes until a strong specific signal. Embryos were then fixed and bleached with hydrogen peroxide to remove pigment before photography.

Recombinant Lin28 protein production

Relevant coding sequences were cloned into the pET28a expression vector. Recombinant Lin28 proteins were expressed overnight at 16°C in B834 *E.coli* cells grown in LB media, following induction with 1 mM IPTG. Cells were harvested by centrifugation and pellets resuspended in a solution containing either 50 mM sodium phosphate pH 7.8, 250 mM NaCl 1 mM DTT, 20 mM imidazole and 10% w/v glycerol (rt-LIN28A); or 50 mM Tris HCL pH 7.5, 500 mM NaCl, 0.5 mM DTT, 20 mM imidazole and 10% w/v sucrose (Xrt-lin28a). The resuspension solution was supplemented with 0.5 µg/mL leupeptin, 0.7 µg/mL pepstatin and 1 mM AEBSF protease inhibitors. Cells were lysed by sonication and the lysate applied to a 5 mL HisTrap column (GE Healthcare). Bound protein was eluted using a linear imidazole gradient (20-500 mM). Fractions containing Lin28 were analysed by SDS-PAGE, pooled, concentrated, and applied to an S200 gel filtration column (GE Healthcare) in a running buffer consisting of either 20 mM Tris pH 7.5, 150 mM NaCl, 1 mM DTT, 10% w/v glycerol (rt-LIN28A) or 10 mM Tris pH 7.5, 150 mM NaCl, 2mM DTT and 10% w/v sucrose (Xrt-lin28a). Eluting fractions containing Lin28 were analyzed by SDS-PAGE, pooled and concentrated, before being flash frozen in liquid N_2 and stored at -80°C. Proteins were produced as N-terminal fusions with the sequence, MGSSHHHHHHSSGLVPRGSHM, containing a His-tag and thrombin digest site. In the case of the human rt-Lin28a, the N-terminal His-tag was removed by thrombin digest prior to gel filtration.

Full-length human LIN28A protein

MGSVSNQQFAGGCAKAAEEAPEEAPEDAARAADEPQLLHGAGICKWFNVRMGFGFLSM
TARAGVALDPPVDVFVHQSKLHMEGFRSLKEGEAVEFTFKKSAKGLESIRVTGPGGVFCI
GSERRPKGKSMQKRRSKGDRCYNCGGLDHHAKECKLPPQPKKCHFCQSISHMVASCPL
KAQQGPSAQGKPTYFREEEEEIHSPTLLPEAQN

N-and C-terminally truncated human LIN28A protein (rt-LIN28A), residues 37-180

LLHGAGICKWFNVRMGFGFLSMTARAGVALDPPVDVFVHQSKLHMEGFRSLKEGEAVEF
TFKKSAKGLESIRVTGPGGVFCIGSERRPKGKSMQKRRSKGDRCYNCGGLDHHAKECKL
PPQPKKCHFCQSISHMVASCPLKAQQ

N-and C-terminally truncated *Xenopus* lin28a protein (Xrt-lin28a), residues 34-177

MGSSHHHHHHSSGLVPRGSHMGSGVCKWFNVRMGFGFLTMTKKEGTDLETPVDVFVH QSKLHMEGFRSLKEGESVEFTFKKSSKGLESTRVTGPGGAPCIGSERRPKVKGQQKRR QKGDRCYNCGGLDHHAKECKLPPQPKKCHFCQSPNHMVAQCPAKASQAAN.

(Leader containing the His-tag and thrombin cleavage site is indicated in bold)

RNA electrophoretic mobility shift assays (EMSAs)

Pre-cursor *mir-363* RNA was synthesised in vitro. DNA templates for *pre-mir-363* were produced by PCR, to include an SP6 RNA polymerase promoter at the beginning of the sequence, using a plasmid containing the *Xenopus* mir-106a-363 as template and the following primers. RNA was synthesised using SP6 Megascript kit (Ambion) according to manufacturer's instructions.

Pre-mir-363

Forward: ATTTAGGTGACACTATAGGGCTGAGGTAGTTGTTT

Reverse: TAGGCAAGGCAGTGGCCTGTACAG

RNA oligonucleotides used in RNA mobility shift assays were synthesised by Dharmacon.

L-mir-138

UUGUGAAUCAGGCCGUGACCACUCAGAAAACGGCUACUUCACAAC

L-mir-363

UGCAAUUUUAUUUAGUUUGGUAGGAGAAAAAUUGC

mL-mir-363

UGCAAUUUUAUUUAGUUUGGUAUGAUAAAAAUUGC

RNA oligonucleotides and mir-RNA precursors were radioactively labelled with ^{32}P ATP using the KinaseMax kit (Ambion) according to manufacturer's instructions.

Recombinant protein EMSAs were performed with the proteins described above. For embryo extract EMSAs, uninjected *X. laevis* controls embryos and embryos injected with 1 ng *lin28a1*, *lin28a2* or *lin28b* mRNA (Faas et al., 2013) were lysed in 50 mM Tris-HCl pH 7.9, 25% glycerol, 50 mM KCl, 2 mM DTT, 0.1 mM EDTA, 1/100 Protease inhibitor cocktail III (Calbiochem)) at 10 µl/embryo. Lysates were cleared by centrifugation and extracts were diluted as required in the lysis buffer.

Binding reactions were carried out as described previously (Piskounova et al., 2008). Labelled RNA probes were incubated with protein in binding buffer (60 mM KCl, 10 mM HEPES, pH 7.6, 3 mM $MgCl_2$, 5% glycerol, 1 mM DTT, 5 µg/µl heparin (Sigma) and 150 ng yeast total RNA competitor (Ambion)) for 30 minutes at room temperature.

The custom anti-lin28a antibody (Enzo Life Sciences (UK) Ltd), used for the embryo extract supershift assays, has been previously described (Faas et al., 2013) and was used at 1/20 dilution per binding reaction, with 1/20 dilution pre-immune bleed used as a serum control. 20 units of RNAsin (Promega) were added per binding. Antibody was pre-incubated with protein and binding buffer for 20 minutes on ice, before labelled probe was added for a further 20 minutes at room temperature.

Samples were run on a 10% native polyacrylamide gel. Gels were dried and exposed either to a Phosphor Screen (GE Healthcare) and were scanned, processed and analysed using a Bio-Rad Molecular FX Imager and Quantity One software (Bio-Rad); or exposed to Hyperfilm ECL film (Amersham) and films analysed using Image J. The proportion of RNA bound at each protein concentration was calculated, and the K_d determined by non-linear regression using the SigmaPlot software package, with the equation:

$$\text{Proportion bound} = \frac{B_{max}\,[\text{lin28}]}{K_d + [\text{lin28}]}$$

Acknowledgements

This work was funded by a BBSRC project grant awarded to HVI (Ref: BB/H000925/1), a BBSRC PhD studentship to FW, HVI & PG (BB/D527026/1) and a YCR PhD studentship to DP, FA & MC (Y001 PhD). We would like to thank Naveed Aziz from the Department of Biology, University of York Technology Facility for his technical assistance with the Affymetrix miRNA array analysis. We would also like to thank Dylan Sweetman for advice on LNA *in situ* hybridisation analysis.

References

Branney Pa, Faas L, Steane SE, Pownall ME, Isaacs HV. 2009. Characterisation of the fibroblast growth factor dependent transcriptome in early development. PloS one 4:e4951-e4951.

de Pontual L, Yao E, Callier P, Faivre L, Drouin V, Cariou S, Van Haeringen A, Genevieve D, Goldenberg A, Oufadem M, Manouvrier S, Munnich A, Vidigal JA, Vekemans M, Lyonnet S, Henrion-Caude A, Ventura A, Amiel J. 2011. Germline deletion of the miR-17 approximately 92 cluster causes skeletal and growth defects in humans. Nat Genet 43:1026-1030.

Faas L, Warrander FC, Maguire R, Ramsbottom SA, Quinn D, Genever P, Isaacs HV. 2013. Lin28 proteins are required for germ layer specification in Xenopus. Development 140:976-986.
Guil S, Caceres JF. 2007. The multifunctional RNA-binding protein hnRNP A1 is required for processing of miR-18a. Nat Struct Mol Biol 14:591-596.
Harland RM. 1991. *In situ* hybridization: An improved whole-mount method for *Xenopus* embryos. Methods in Cell Biology 36:685-695.
Heo I, Joo C, Cho J, Ha M, Han J, Kim VN. 2008. Lin28 mediates the terminal uridylation of let-7 precursor MicroRNA. Molecular cell 32:276-284.
Heo I, Joo C, Kim YK, Ha M, Yoon MJ, Cho J, Yeom KH, Han J, Kim VN. 2009. TUT4 in concert with Lin28 suppresses microRNA biogenesis through pre-microRNA uridylation. Cell 138:696-708.
Khokha MK, Yeh J, Grammer TC, Harland RM. 2005. Depletion of three BMP antagonists from Spemann's organizer leads to a catastrophic loss of dorsal structures. Dev Cell 8:401-411.
Marcelis CL, Hol FA, Graham GE, Rieu PN, Kellermayer R, Meijer RP, Lugtenberg D, Scheffer H, van Bokhoven H, Brunner HG, de Brouwer AP. 2008. Genotype-phenotype correlations in MYCN-related Feingold syndrome. Hum Mutat 29:1125-1132.
Mayr F, Heinemann U. 2013. Mechanisms of Lin28-mediated miRNA and mRNA regulation--a structural and functional perspective. Int J Mol Sci 14:16532-16553.
Mendell JT. 2008. miRiad roles for the miR-17-92 cluster in development and disease. Cell 133:217-222.
Michlewski G, Caceres JF. 2010. Antagonistic role of hnRNP A1 and KSRP in the regulation of let-7a biogenesis. Nat Struct Mol Biol 17:1011-1018.
Mogilyansky E, Rigoutsos I. 2013. The miR-17/92 cluster: a comprehensive update on its genomics, genetics, functions and increasingly important and numerous roles in health and disease. Cell Death Differ 20:1603-1614.
Moss EG, Lee RC, Ambros V. 1997. The cold shock domain protein LIN-28 controls developmental timing in C. elegans and is regulated by the lin-4 RNA. Cell 88:637-646.
Olive V, Jiang I, He L. 2010. mir-17-92, a cluster of miRNAs in the midst of the cancer network. The international journal of biochemistry & cell biology 42:1348-1354.
Ouchi Y, Yamamoto J, Iwamoto T. 2014. The heterochronic genes lin-28a and lin-28b play an essential and evolutionarily conserved role in early zebrafish development. PLoS One 9:e88086.
Piskounova E, Viswanathan SR, Janas M, LaPierre RJ, Daley GQ, Sliz P, Gregory RI. 2008. Determinants of microRNA processing inhibition by the developmentally regulated RNA-binding protein Lin28. The Journal of biological chemistry 283:21310-21314.
Reece-Hoyes JS, Keenan ID, Isaacs HV. 2002. Cloning and expression of the Cdx family from the frog Xenopus tropicalis. Developmental dynamics : an official publication of the American Association of Anatomists 223:134-140.
Shyh-Chang N, Daley GQ. 2013. Lin28: primal regulator of growth and metabolism in stem cells. Cell Stem Cell 12:395-406.
Shyh-Chang N, Zhu H, Yvanka de Soysa T, Shinoda G, Seligson MT, Tsanov KM, Nguyen L, Asara JM, Cantley LC, Daley GQ. 2013. Lin28 enhances tissue repair by reprogramming cellular metabolism. Cell 155:778-792.
Sweetman D. 2011. In situ detection of microRNAs in animals. Methods Mol Biol 732:1-8.
Sweetman D, Rathjen T, Jefferson M, Wheeler G, Smith TG, Wheeler GN, Munsterberg A, Dalmay T. 2006. FGF-4 signaling is involved in mir-206 expression in developing somites of chicken embryos. Dev Dyn 235:2185-2191.

Vadla B, Kemper K, Alaimo J, Heine C, Moss EG. 2012. lin-28 controls the succession of cell fate choices via two distinct activities. PLoS Genet 8:e1002588.
Ventura A, Young AG, Winslow MM, Lintault L, Meissner A, Erkeland SJ, Newman J, Bronson RT, Crowley D, Stone JR, Jaenisch R, Sharp PA, Jacks T. 2008. Targeted deletion reveals essential and overlapping functions of the miR-17 through 92 family of miRNA clusters. Cell 132:875-886.
Viswanathan SR. 2008. Selective Blockade of MicroRNA. In Vitro 97.
Viswanathan SR, Daley GQ. 2010. Lin28: A microRNA regulator with a macro role. cell 140:445-449.
Viswanathan SR, Daley GQ, Gregory RI. 2008. Selective blockade of microRNA processing by Lin28. Science (New York, N.Y.) 320:97-100.
Wilson KD, Venkatasubrahmanyam S, Jia F, Sun N, Butte AJ, Wu JC. 2009. MicroRNA profiling of human-induced pluripotent stem cells. Stem Cells Dev 18:749-758.
Winterbottom EF, Illes JC, Faas L, Isaacs HV. 2010. Conserved and novel roles for the Gsh2 transcription factor in primary neurogenesis. development 137:2623-2631.

Figure Legends

Figure 1

A, Western blot analysis of endogenous lin28a and lin28b expression in embryos injected with a total of 12.5 ng/embryo of lin28 MOs in the compound knockdown compared to CMO injected and uninjected control embryos at stage 16. GAPDH was used as a loading control.

B, Scale diagram showing the genomic organisation of *Xenopus* mir-17~92 and mir-106~363 clusters. Coloured boxes indicate pre-miRNA sequences, with each colour corresponding to paralog groupings based on seed sequence. Where known, the black and grey boxes, respectively, represent the major and minor forms derived from a common precursor.

C, qRT-PCR was performed on embryos injected with 10 ng each/embryo of lin28a1, a2 and b MOs and control embryos, at stage 10.5. Fold change in expression of miRNAs is shown compared to controls and normalised using U6 by the 2-ΔΔCt method. Fold change is given as average of 3 biological replicates, with error bars representing SE.

D, Predicted secondary structure of *Xenopus pre-mir-363.* The sequences of mature *mir-363-5p, mir-363-3p* and the putative lin28 binding site are indicated.

Figure 2

A, Western blot analysis of overexpressed lin28 proteins at stage 10.5 in control embryos and embryos injected with 1 ng of mRNAs coding for either lin28a1, lin28a2 or lin28b. GAPDH was used as a loading control.

B, Phenotype of control embryos and embryos overexpressing either lin28a1, lin28a2 or lin28b at stage 38.

C, qRT-PCR was performed on embryos injected with control embryos and either 1 ng of mRNAs coding for lin28a1, a2 or b MOs at stage 10.5. Fold change in expression of miRNAs is shown compared to controls and normalised using U6 by the 2-ΔΔCt method. Fold change is given as average of 3 biological replicates, with error bars representing SE.

Figure 3

A, Scale diagram of the *Xenopus* proteins used in this study. Cold shock domains are shaded magenta and zinc knuckles green.

B, EMSA performed with ^{32}P-labelled L-let-7g and indicated concentrations of human recombinant LIN28A protein, either full-length or truncated (rt). Arrows indicate labelled RNA (blue) and LIN28A-RNA complex (red).

C, EMSA performed with ^{32}P-labelled L-let-7g and indicated concentrations of Xrt-lin28a. Gel shown is representative of n=3. Arrows indicate labelled RNA (blue) and lin28-RNA complex (red). Band intensities were quantified from three independent experiments and the proportion bound was calculated. Data were fit by non-linear regression as described in Materials and Methods. B_{max} = 1.017.

D, EMSA performed with ^{32}P-labelled L-mir-138 and indicated concentrations of Xrt-lin28a. Arrows indicate RNA and lin28a-RNA complex. Gel shown is representative of n=3. Arrows indicate labelled RNA (blue) and lin28-RNA complex (red).

Figure 4

A, EMSA performed with ^{32}P-labelled L-mir-363 and indicated concentrations of Xrt-lin28a. Gel shown is representative of n=3. Band intensities were quantified from three independent experiments and the proportion bound was calculated. Data were fit by non-linear regression as described in *Materials and Methods*. Bmax = 0.962.

B, EMSA performed with ^{32}P-labelled L-mir-363 and 1 μM of Xrt-lin28a (except for RNA only lane). Arrows indicate RNA and lin28a-RNA complex. Reactions were competed with unlabelled RNA of L-mir-363 or L-mir-138 in excess levels as indicated. Band intensities were quantified and proportion of RNA bound was calculated. Gel shown is representative of n=2. Arrows indicate labelled RNA (blue) and lin28-RNA complex (red).

C, EMSA performed with ^{32}P-labelled mL-mir-363 and indicated concentrations of Xrt-lin28a. Gel shown is representative of n=3.

Figure 5

A and B, EMSAs performed with ^{32}P-labelled L-mir-363 and embryo extract from uninjected controls or embryos injected with 1 ng of either A) *lin28a1* or B) *lin28a2*. Embryo extract was used at 1/16 dilution for lanes 2-3, 5-6, and at 1/32 dilution for lower concentration of overexpressing extract in lane 4. Arrows indicate unbound RNA (blue), lin28-RNA complex (red), and supershift complex of antibody-lin28-RNA (green). +Ab = 1/20 dilution α-lin28a, +ser = 1/20 dilution pre-immune bleed serum, both incubated with protein on ice for 20 minutes before addition of probe.

C and D, EMSAs performed with ^{32}P-labelled *pre-mir-363* and embryo extract from uninjected controls or embryos injected with 1 ng of either C) *lin28a1* or D) *lin28a2*. Embryo extract was used at 1/8 dilution for lanes 2-3, 5-6, and at 1/16 dilution for lower concentration of overexpressing extract in lane 4. Arrows indicate unbound RNA (blue), lin28-RNA complex (red), and supershift complex of antibody-lin28-RNA (green). +Ab = 1/20 dilution α-lin28a , +ser = 1/20 dilution pre-immune bleed serum, both incubated with protein on ice for 20 minutes before addition of probe.

Figure 6

A, Developmental time course for expression of *pri-miR-17~92* and *pri-miR-106~363* was undertaken using RT-PCR. *L8* was used as a loading control. Image is representative of n=2. *miR-17-92* = 669 bp, *miR-106-363* = 639 bp, *L8* = 435 bp.

B, *In situ* hybridisations showing expression of *pri-miR-17~92* and *pri-miR-106~363* RNAs in early development. Vegetal views of early gastrula stage 10.5 embryos, with the dorsal side is to the top. Arrows indicate the dorsal blastopore lip.

C, *In situ* hybridisation using an anti-sense LNA probe showing *mir-363-3p* expression in early development. Vegetal views of gastrula stages 10 and 10.5 are shown, with dorsal-side to the top. An animal to vegetal bisect of a stage 10 embryo is shown with the animal hemisphere to the top and dorsal to the right. A dorsal view of a late neurula stage 19 embryo, anterior to the left. Plane of bisection (black line), dorsal blastopore lip (bl) and neural plate (np) are indicated.

D, *In situ* hybridisation using an anti-sense LNA probe showing *mir-363-5p* expression in early development. Vegetal views of gastrula stages 10 and 11 are shown, with dorsal-side to the top. An animal to vegetal bisect of a stage 10 embryo is shown with the animal hemisphere to the top and dorsal to the right. A dorsal view of a late neurula stage 19 embryo, anterior to the left. Plane of bisection (black line) is indicated.

Tables

Table 1- Changes in miRNA expression in late gastrula stage 13 lin28 morphant embryos

The expression of *Xenopus* miRNAs in lin28 morphants and control embryos at late gastrula stage 13. Expression levels are shown as ratios relative to abundance in a mixed stage reference RNA sample. Only miRNAs flagged as being detected in all three replicate arrays are included. miRNAs showing ≥2 fold change and p≤0.05 are shaded in grey. Memberships of mir-106~363 and mir-17~92 clusters are indicated.

miRNA	Mean Control	Mean AMO	Fold Change in Morphant Relative to Control	Member of mir-106~363 Cluster	Member of mir-17~92 Cluster
xtr-miR-20a	1.50	0.51	-2.9		X
xtr-miR-17-5p	1.26	0.52	-2.4		X
xtr-miR-200a	1.25	0.59	-2.1		
xtr-miR-20b	1.29	0.61	-2.1	X	
xtr-miR-301	1.14	0.54	-2.1		
xtr-miR-363-3p	1.28	0.60	-2.1	X	
xtr-miR-19a	1.36	0.67	-2.0		X
xtr-miR-19b	1.27	0.63	-2.0	X	
xtr-miR-428	1.27	0.63	-2.0		
xtr-miR-200b	1.37	0.71	-1.9		
xtr-miR-130b	1.32	0.86	-1.5		
xtr-miR-203	1.14	0.75	-1.5		
xtr-miR-30b	1.13	0.90	-1.3		
xtr-miR-125a	1.27	1.11	-1.1		
xtr-miR-126	2.46	2.43	-1.0		
xtr-miR-427	1.09	1.04	-1.0		
xtr-let-7c	1.10	1.20	-0.9		
xtr-let-7a	1.16	1.14	1.0		
xtr-let-7e	0.97	0.99	1.0		
xtr-miR-155	1.09	1.15	1.1		
xtr-miR-22	0.92	1.00	1.1		
xtr-miR-7	0.93	1.27	1.4		

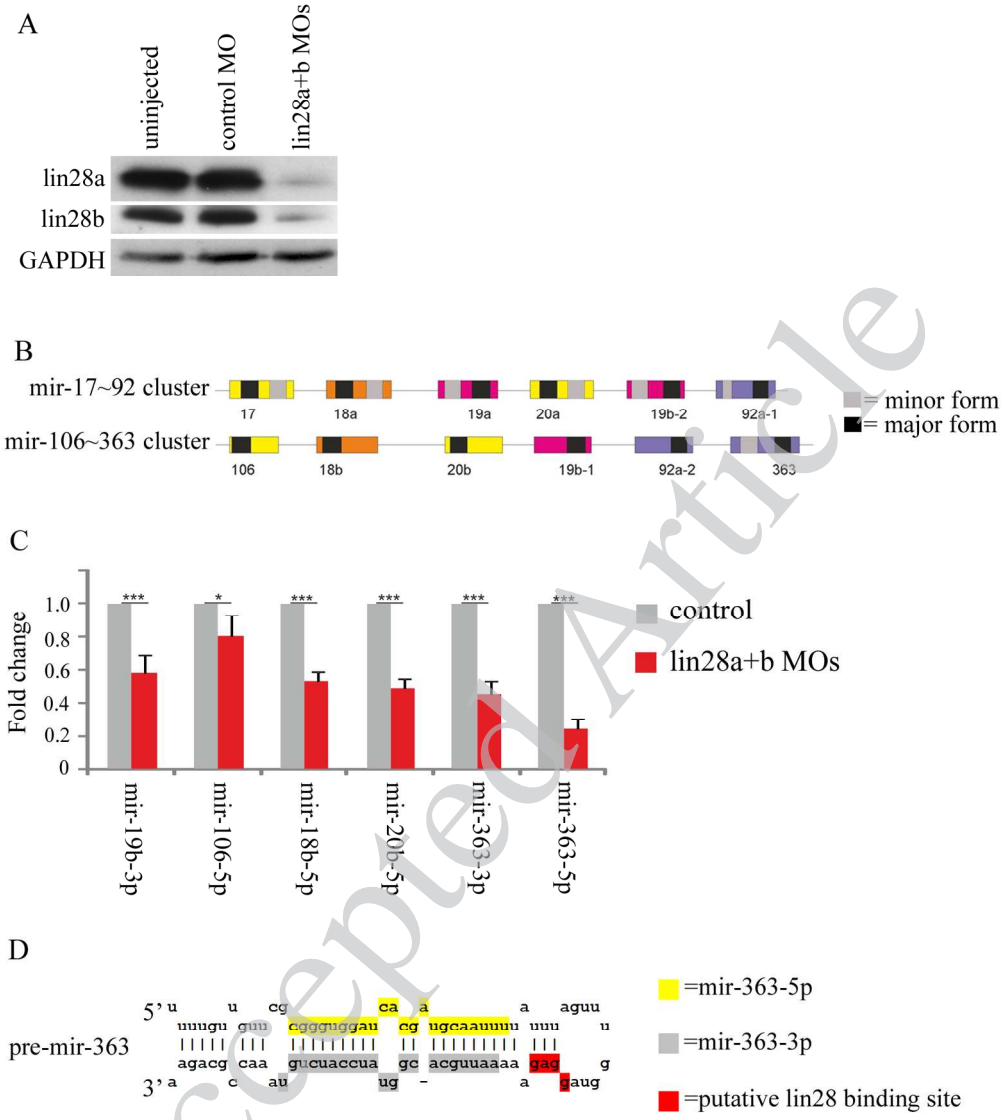

168x191mm (300 x 300 DPI)

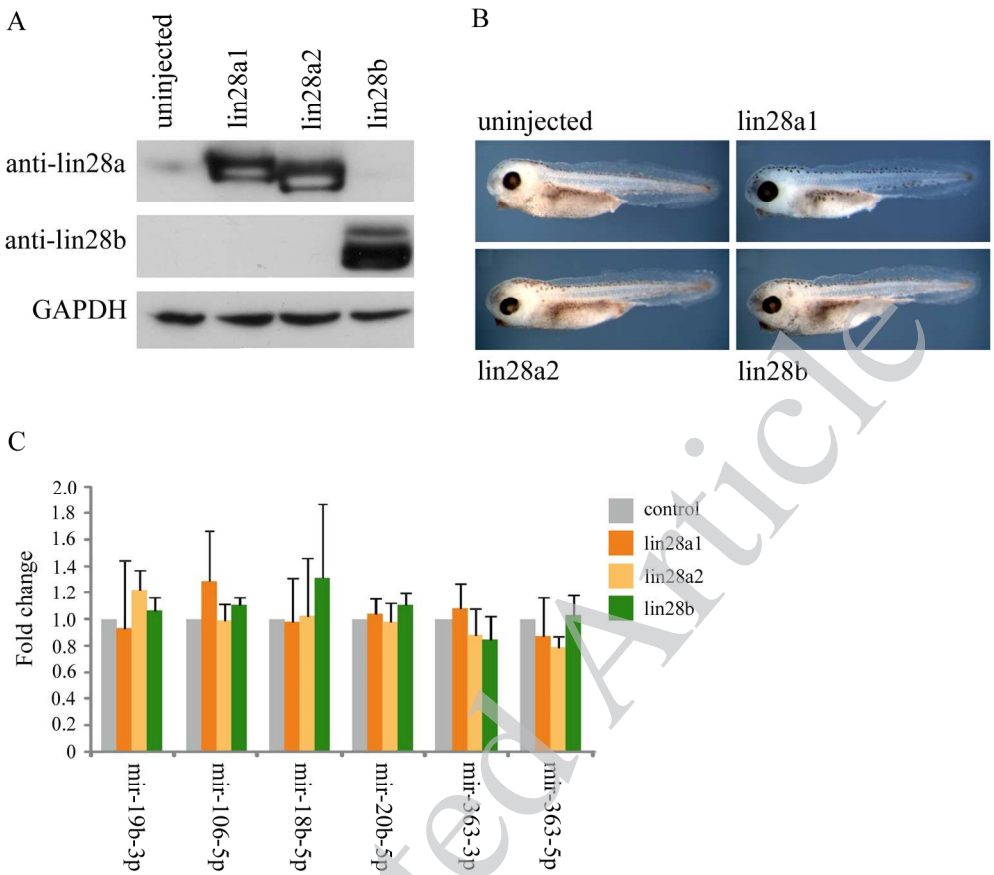

177x155mm (300 x 300 DPI)

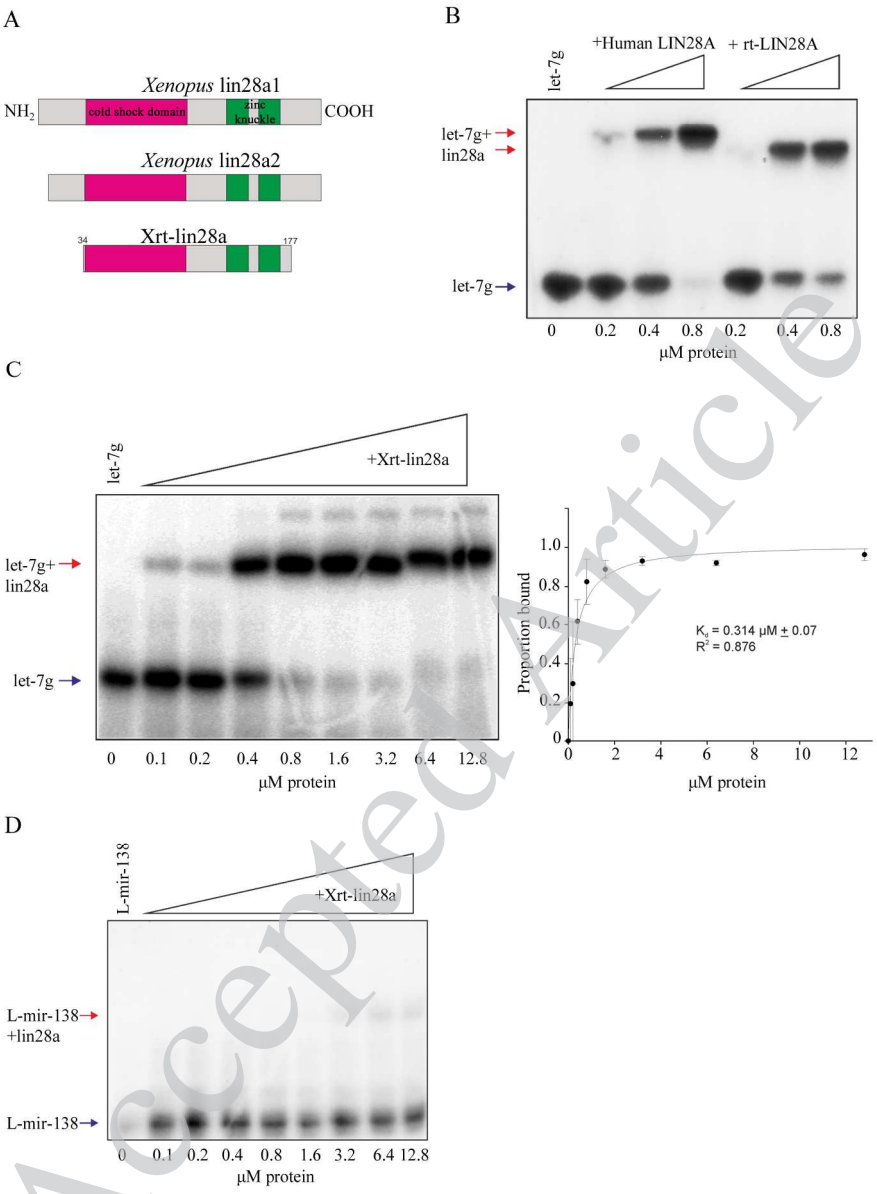

177x243mm (300 x 300 DPI)

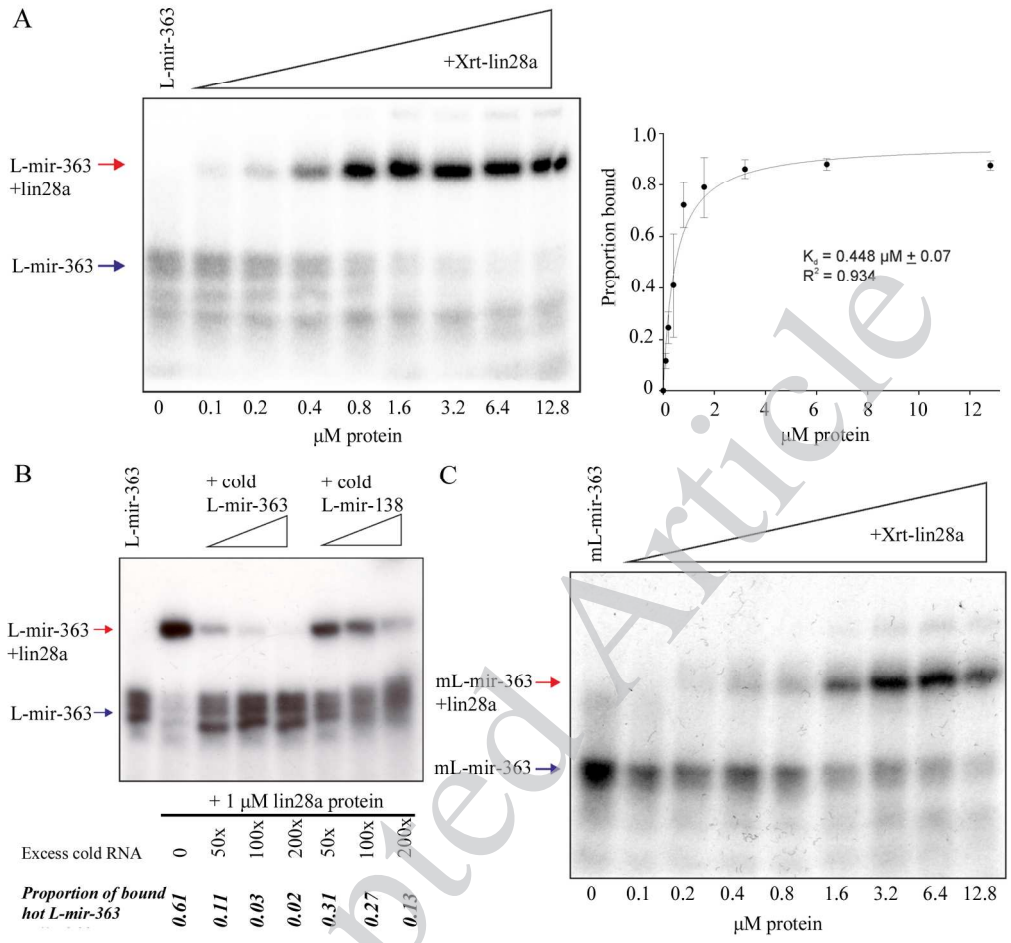

177x175mm (300 x 300 DPI)

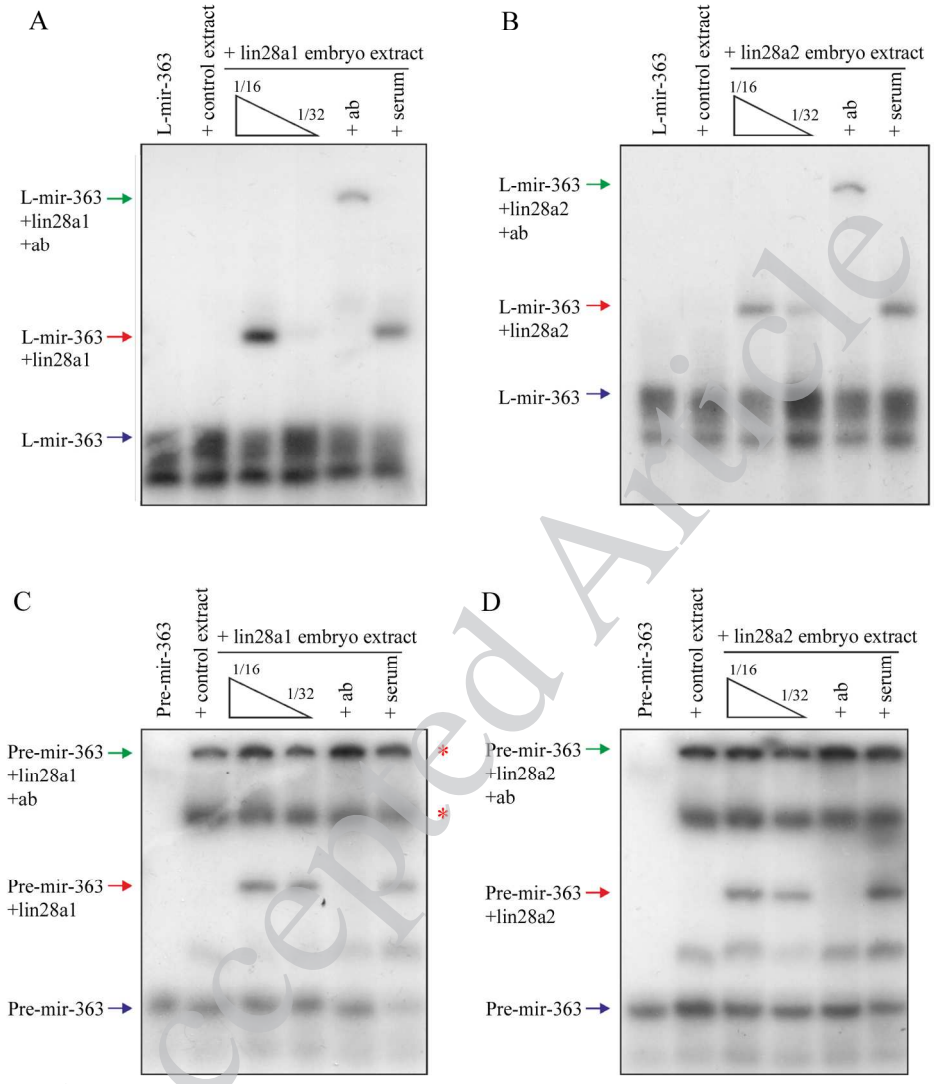

177x207mm (300 x 300 DPI)

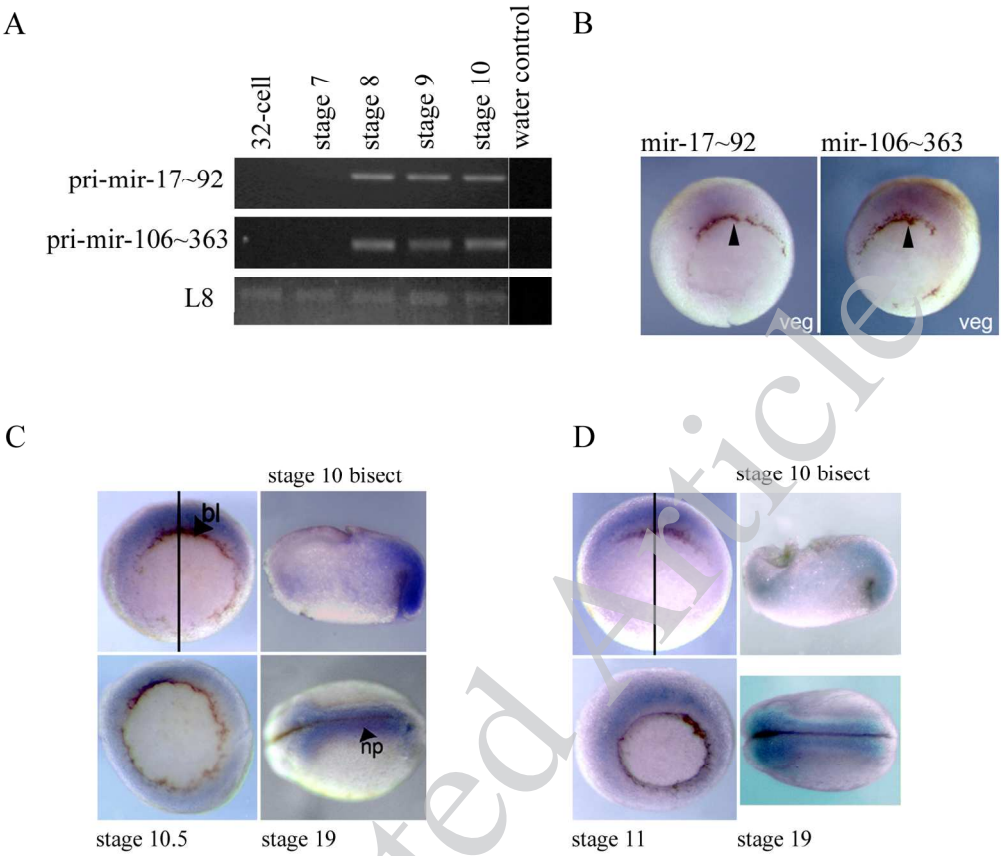

ProbeSet Name	Xt Control s	p-value (Xt	Detection (	Xt Control s	p-value (Xt	Detection (	Xt Control s
xla-miR-133a_st	-6.98832	0.253597	FALSE	-5.59715	0.314792	FALSE	-21.2993
xla-miR-18_st	6.25589	3.99E-06	TRUE	6.284979	7.98E-07	TRUE	5.911086
xla-miR-19b_st	8.021943	2.05E-08	TRUE	8.586702	2.05E-08	TRUE	8.689745
xla-miR-20_st	10.15411	2.05E-08	TRUE	9.611137	2.05E-08	TRUE	9.500816
xla-miR-427_st	8.925426	2.05E-08	TRUE	10.30349	2.05E-08	TRUE	10.07677
xla-miR-428_st	-19.579	0.569927	FALSE	1.406357	0.18587	FALSE	-41.2861
xla-miR-429_st	-19.76	0.091179	FALSE	-20.9308	0.299153	FALSE	1.182627
xtr-let-7a_st	-43.1851	0.913198	FALSE	-42.5378	0.911371	FALSE	-42.5378
xtr-let-7b_st	1.115331	0.31696	FALSE	1.156406	0.454202	FALSE	1.287783
xtr-let-7c_st	-18.7449	0.067533	FALSE	-21.9844	0.8921	FALSE	-21.515
xtr-let-7e_st	-31.9919	0.613948	FALSE	-31.4531	0.457195	FALSE	-32.6485
xtr-let-7f_st	-43.1851	0.83393	FALSE	-42.4781	0.96685	FALSE	-42.4781
xtr-let-7g_st	-43.1851	0.960144	FALSE	-22.6032	0.686109	FALSE	-43.1851
xtr-let-7i_st	-42.5366	0.677161	FALSE	2.597015	0.079986	FALSE	-43.1851
xtr-miR-100_st	-10.4172	0.420589	FALSE	1.70085	0.139918	FALSE	-8.4206
xtr-miR-101a_st	-14.0781	0.469169	FALSE	-14.6398	0.760154	FALSE	-43.1851
xtr-miR-103_st	4.890649	0.000124	TRUE	4.449744	0.001372	TRUE	4.564379
xtr-miR-106_st	10.02694	2.05E-08	TRUE	9.86487	2.05E-08	TRUE	9.397475
xtr-miR-107_st	4.854665	0.000451	TRUE	5.000524	0.000209	TRUE	4.874667
xtr-miR-10a_st	-7.82008	0.138049	FALSE	-8.31858	0.258003	FALSE	-12.6441
xtr-miR-10b_st	-2.337	0.347107	FALSE	-2.57465	0.386082	FALSE	-41.9579
xtr-miR-10c_st	-23.2522	0.254994	FALSE	-43.1851	0.981367	FALSE	-0.47161
xtr-miR-122_st	-20.0232	0.332865	FALSE	-20.9302	0.741187	FALSE	-21.3391
xtr-miR-124_st	3.965301	0.001104	TRUE	4.894166	0.000692	TRUE	3.091718
xtr-miR-125a_st	-21.2263	0.542505	FALSE	-43.1851	0.738736	FALSE	-20.1745
xtr-miR-125b_st	0.675224	0.252807	FALSE	1.977129	0.075636	FALSE	0.717267
xtr-miR-126_st	-19.8254	0.320235	FALSE	2.591275	0.021122	TRUE	3.782233
xtr-miR-126-star_st	-21.5516	0.605431	FALSE	-20.6566	0.682679	FALSE	-22.7864
xtr-miR-128_st	1.092583	0.307485	FALSE	2.389263	0.152081	FALSE	2.599521
xtr-miR-129_st	2.102314	0.046172	TRUE	2.884414	0.096091	FALSE	3.658851
xtr-miR-130a_st	4.933491	0.000208	TRUE	3.993314	0.000728	TRUE	4.564212
xtr-miR-130b_st	6.837008	5.08E-07	TRUE	6.756852	5.57E-07	TRUE	5.489235
xtr-miR-130c_st	4.122761	0.000263	TRUE	0.562932	0.234354	FALSE	2.36566
xtr-miR-132_st	-20.429	0.257256	FALSE	-1.14482	0.529082	FALSE	-21.2088
xtr-miR-133a_st	-43.0233	0.793191	FALSE	-29.879	0.42459	FALSE	-29.6094
xtr-miR-133b_st	-43.1851	0.736217	FALSE	-40.3379	0.936667	FALSE	-26.3396
xtr-miR-133c_st	0.614309	0.233469	FALSE	2.231741	0.106382	FALSE	0.177374
xtr-miR-133d_st	1.971693	0.067931	FALSE	3.488738	0.03526	TRUE	4.131734
xtr-miR-135_st	-21.9328	0.685877	FALSE	1.646982	0.183686	FALSE	-2.41092
xtr-miR-137_st	2.036124	0.330934	FALSE	-0.17377	0.528451	FALSE	-0.58267
xtr-miR-138_st	-43.1851	0.999407	FALSE	1.110741	0.359709	FALSE	-43.1851
xtr-miR-139_st	-22.0585	0.503979	FALSE	-11.6743	0.374543	FALSE	-6.93512
xtr-miR-140_st	1.655217	0.024244	TRUE	2.106423	0.00861	TRUE	1.732523
xtr-miR-142-3p_st	-11.9385	0.340133	FALSE	-11.5695	0.838377	FALSE	-11.9569
xtr-miR-142-5p_st	-15.3107	0.29936	FALSE	1.170469	0.052098	TRUE	-1.44992
xtr-miR-143_st	-43.1851	0.81287	FALSE	-20.8729	0.553766	FALSE	1.915251

xtr-miR-144_st	-10.6902	0.40928	FALSE	-12.2189	0.792805	FALSE	-11.6607
xtr-miR-145_st	1.911211	0.23923	FALSE	1.522311	0.466716	FALSE	2.16213
xtr-miR-146_st	-22.6209	0.834296	FALSE	-8.67492	0.675783	FALSE	-24.3897
xtr-miR-146b_st	1.742314	0.140523	FALSE	1.055602	0.141366	FALSE	3.443619
xtr-miR-148a_st	-20.0301	0.159291	FALSE	2.64733	0.036267	TRUE	4.269605
xtr-miR-148b_st	-43.1851	0.541819	FALSE	-19.6585	0.24097	FALSE	1.217563
xtr-miR-150_st	2.225047	0.07556	FALSE	2.675978	0.014412	TRUE	2.731841
xtr-miR-153_st	-21.4104	0.659387	FALSE	-22.6294	0.252939	FALSE	-20.4554
xtr-miR-155_st	-20.4476	0.028829	TRUE	0.469082	0.045995	TRUE	0.539803
xtr-miR-15a_st	-21.2537	0.143788	FALSE	4.033212	0.001528	TRUE	2.833105
xtr-miR-15b_st	1.633215	0.007582	TRUE	-19.2806	0.010913	TRUE	5.296054
xtr-miR-15c_st	3.908887	0.006617	TRUE	5.144438	2.38E-06	TRUE	4.502397
xtr-miR-16a_st	0.472575	0.110791	FALSE	3.374022	0.001578	TRUE	2.42432
xtr-miR-16b_st	5.522696	2.46E-06	TRUE	6.622447	2.05E-08	TRUE	6.636358
xtr-miR-16c_st	7.66024	2.05E-08	TRUE	7.846328	2.47E-07	TRUE	7.735746
xtr-miR-17-3p_st	4.343112	0.000425	TRUE	4.010185	0.001363	TRUE	2.224097
xtr-miR-17-5p_st	8.55098	2.05E-08	TRUE	8.622456	2.05E-08	TRUE	8.429112
xtr-miR-181a_st	2.609154	0.030634	TRUE	2.872095	0.029955	TRUE	-19.3295
xtr-miR-181a-1-star_st	-11.5021	0.482025	FALSE	-10.802	0.45481	FALSE	-13.3054
xtr-miR-181a-2-star_st	4.153307	0.002676	TRUE	3.875835	0.017756	TRUE	3.117788
xtr-miR-181b_st	4.197134	0.000911	TRUE	4.403922	0.000807	TRUE	4.606293
xtr-miR-182_st	-31.829	0.647067	FALSE	-32.4522	0.775874	FALSE	-31.7549
xtr-miR-182-star_st	0.089682	0.314438	FALSE	1.48679	0.058884	TRUE	-13.1192
xtr-miR-183_st	-42.9462	0.887142	FALSE	-2.30174	0.74118	FALSE	-43.1851
xtr-miR-184_st	-0.88672	0.282097	FALSE	-21.2492	0.159694	FALSE	-1.99188
xtr-miR-187_st	0.359739	0.361016	FALSE	-39.8588	0.90815	FALSE	-39.8588
xtr-miR-189_st	1.661299	0.074679	FALSE	-27.112	0.276445	FALSE	-27.9057
xtr-miR-18a_st	7.936952	2.05E-08	TRUE	7.694314	2.47E-07	TRUE	7.321966
xtr-miR-18a-star_st	4.306341	0.000391	TRUE	5.421235	4.25E-05	TRUE	4.024499
xtr-miR-18b_st	6.32013	1.63E-06	TRUE	5.961141	1.14E-06	TRUE	5.545242
xtr-miR-191_st	2.245372	0.112608	FALSE	3.925025	0.008859	TRUE	3.363569
xtr-miR-192_st	-11.7903	0.189193	FALSE	1.341266	0.181587	FALSE	-12.0375
xtr-miR-193_st	-8.91722	0.40011	FALSE	-12.1823	0.421313	FALSE	-9.42723
xtr-miR-194_st	-7.16454	0.496056	FALSE	-23.0723	0.890242	FALSE	-4.57894
xtr-miR-196a_st	-0.46347	0.24282	FALSE	-0.85959	0.575772	FALSE	-42.6565
xtr-miR-196b_st	-34.6924	0.643798	FALSE	-20.9834	0.699763	FALSE	-33.9836
xtr-miR-199a_st	-21.33	0.723077	FALSE	-34.8504	0.476103	FALSE	-34.1869
xtr-miR-199a-star_st	1.833323	0.355819	FALSE	-11.6391	0.249566	FALSE	-24.8181
xtr-miR-199b_st	-10.8831	0.171197	FALSE	-14.9591	0.381494	FALSE	2.427896
xtr-miR-19a_st	2.826518	0.005196	TRUE	3.878643	0.000688	TRUE	1.362904
xtr-miR-19b_st	7.799026	2.05E-08	TRUE	8.484215	2.05E-08	TRUE	8.60972
xtr-miR-1a_st	-43.1851	0.603262	FALSE	-43.1851	0.735925	FALSE	-42.5235
xtr-miR-1b_st	-43.1851	0.814758	FALSE	-16.8237	0.370899	FALSE	-37.3207
xtr-miR-200a_st	-39.5711	0.093212	FALSE	-39.7445	0.47337	FALSE	-40.7383
xtr-miR-200b_st	-20.3686	0.417305	FALSE	3.1542	0.065593	FALSE	-11.25
xtr-miR-202_st	4.601694	0.000751	TRUE	4.422277	0.009673	TRUE	3.972862
xtr-miR-202-star_st	-0.1401	0.055861	TRUE	-43.1851	0.987407	FALSE	-2.38775

xtr-miR-203_st	-42.8901	0.890264	FALSE	1.495072	0.327604	FALSE	-42.8901
xtr-miR-204_st	3.354398	0.005971	TRUE	-19.778	0.49589	FALSE	3.384656
xtr-miR-205a_st	2.518052	0.020306	TRUE	-20.0389	0.253508	FALSE	2.940435
xtr-miR-205b_st	-20.7804	0.330781	FALSE	-19.1949	0.172814	FALSE	-21.6606
xtr-miR-206_st	1.742314	0.053593	TRUE	1.449265	0.227923	FALSE	1.344734
xtr-miR-208_st	-43.0724	0.745	FALSE	-43.0724	0.868608	FALSE	-43.0724
xtr-miR-20a_st	9.419922	2.05E-08	TRUE	9.483311	2.05E-08	TRUE	9.399622
xtr-miR-20a-star_st	-0.39559	0.518729	FALSE	-19.3689	0.387765	FALSE	-43.1851
xtr-miR-20b_st	9.818848	2.05E-08	TRUE	9.494179	2.05E-08	TRUE	9.48792
xtr-miR-210_st	3.22981	0.047233	TRUE	1.598242	0.268449	FALSE	-19.2875
xtr-miR-212_st	-20.7938	0.545743	FALSE	-28.8887	0.579874	FALSE	-5.46495
xtr-miR-214_st	7.004673	2.05E-08	TRUE	6.749572	2.47E-07	TRUE	7.323556
xtr-miR-215_st	-6.64954	0.124024	FALSE	-11.1178	0.708872	FALSE	-27.16
xtr-miR-216_st	1.178756	0.2651	FALSE	-2.18845	0.527434	FALSE	-42.328
xtr-miR-217_st	-11.1579	0.559926	FALSE	-10.1587	0.382688	FALSE	-10.2519
xtr-miR-218_st	-20.636	0.019581	TRUE	0.111282	0.01231	TRUE	-43.1851
xtr-miR-219_st	-28.8347	0.785327	FALSE	-28.4997	0.572814	FALSE	-28.8347
xtr-miR-22_st	5.793598	7.36E-06	TRUE	5.650121	7.51E-05	TRUE	5.432227
xtr-miR-221_st	-22.2122	0.449749	FALSE	-22.2122	0.667892	FALSE	-21.9777
xtr-miR-222_st	3.841873	0.003812	TRUE	2.467242	0.091794	FALSE	1.47846
xtr-miR-223_st	4.306408	6.80E-05	TRUE	4.053267	0.000271	TRUE	4.349489
xtr-miR-22-star_st	-43.1851	0.599987	FALSE	-1.2221	0.57353	FALSE	-42.8546
xtr-miR-23a_st	1.842909	0.068684	FALSE	3.019702	0.020466	TRUE	1.348745
xtr-miR-23b_st	5.637318	1.53E-05	TRUE	5.169053	0.000209	TRUE	4.865611
xtr-miR-24a_st	5.493119	1.06E-05	TRUE	5.581633	0.000138	TRUE	5.718351
xtr-miR-24b_st	1.528581	0.143807	FALSE	-19.5714	0.212697	FALSE	1.225013
xtr-miR-25_st	-21.1504	0.354957	FALSE	-1.36566	0.501669	FALSE	-2.2513
xtr-miR-26_st	-19.5384	0.009931	TRUE	4.451858	3.52E-05	TRUE	4.047411
xtr-miR-27a_st	-42.2859	0.623465	FALSE	-42.2859	0.465502	FALSE	-21.8873
xtr-miR-27b_st	-0.62034	0.126924	FALSE	2.306574	0.182914	FALSE	2.92248
xtr-miR-27c_st	-43.1851	0.799026	FALSE	-0.80232	0.34315	FALSE	-31.2695
xtr-miR-29a_st	-43.1714	0.874035	FALSE	-43.1851	0.728724	FALSE	-22.7728
xtr-miR-29b_st	-32.2715	0.617324	FALSE	-21.358	0.299992	FALSE	-32.2715
xtr-miR-29c_st	-32.2584	0.83421	FALSE	-10.4314	0.789356	FALSE	-43.1851
xtr-miR-29c-star_st	-35.519	0.326049	FALSE	-43.1851	0.846086	FALSE	-43.1851
xtr-miR-29d_st	-43.1851	0.954635	FALSE	-43.1851	0.967762	FALSE	-43.1851
xtr-miR-301_st	0.697449	0.11538	FALSE	2.917092	0.113506	FALSE	1.344314
xtr-miR-302_st	-1.59861	0.361753	FALSE	-0.87211	0.1628	FALSE	-1.56073
xtr-miR-30a-3p_st	-43.1851	0.941784	FALSE	-30.2796	0.682176	FALSE	-30.2796
xtr-miR-30a-5p_st	-12.4674	0.475212	FALSE	3.49716	0.02058	TRUE	2.11918
xtr-miR-30b_st	5.027115	2.30E-06	TRUE	5.400769	2.10E-06	TRUE	5.60733
xtr-miR-30c_st	5.460691	0.000192	TRUE	5.710873	1.15E-05	TRUE	6.069403
xtr-miR-30d_st	4.437337	0.002729	TRUE	3.026892	0.033015	TRUE	4.931851
xtr-miR-30e_st	2.14112	0.065628	FALSE	1.763947	0.119887	FALSE	2.820646
xtr-miR-31_st	-13.2597	0.051451	TRUE	-6.48837	0.044686	TRUE	-36.5567
xtr-miR-31b_st	-8.46399	0.207983	FALSE	-20.5782	0.491864	FALSE	-8.19172
xtr-miR-320_st	1.760649	0.073008	FALSE	1.159685	0.112382	FALSE	-19.7027

xtr-miR-338_st	-43.1851	0.659732	FALSE	-43.1851	0.537892	FALSE	-43.1851
xtr-miR-33a_st	-0.50575	0.140729	FALSE	0.611775	0.627862	FALSE	-0.62322
xtr-miR-33b_st	-43.1851	0.903863	FALSE	-17.3292	0.890039	FALSE	-15.8682
xtr-miR-34a_st	0.851965	0.306862	FALSE	-14.8419	0.771206	FALSE	-15.3205
xtr-miR-34b_st	-21.7382	0.551892	FALSE	-15.5399	0.652571	FALSE	-0.94615
xtr-miR-363-3p_st	5.864161	2.47E-07	TRUE	6.528676	2.05E-08	TRUE	6.30936
xtr-miR-363-5p_st	8.18865	2.05E-08	TRUE	7.962089	2.05E-08	TRUE	7.359931
xtr-miR-365_st	-11.8494	0.265558	FALSE	-0.68871	0.111122	FALSE	1.489625
xtr-miR-367_st	4.001463	0.001133	TRUE	1.661289	0.018307	TRUE	2.360147
xtr-miR-375_st	-43.1851	0.735826	FALSE	-33.1551	0.957659	FALSE	-20.9599
xtr-miR-383_st	-0.31723	0.204758	FALSE	-2.1291	0.714219	FALSE	-5.29
xtr-miR-425-5p_st	1.049943	0.154514	FALSE	0.272627	0.367557	FALSE	1.269603
xtr-miR-427_st	9.431849	2.05E-08	TRUE	10.76321	2.05E-08	TRUE	10.57487
xtr-miR-428_st	1.508406	0.085568	FALSE	1.993917	0.184174	FALSE	-2.38774
xtr-miR-429_st	3.014155	0.003153	TRUE	2.5852	0.010931	TRUE	1.8721
xtr-miR-449_st	0.669682	0.380109	FALSE	-19.7914	0.66927	FALSE	-29.4618
xtr-miR-451_st	2.341424	0.058186	TRUE	0.774553	0.133496	FALSE	1.91525
xtr-miR-455_st	2.376502	0.136218	FALSE	2.368785	0.085216	FALSE	3.068942
xtr-miR-489_st	-9.49888	0.036686	TRUE	-12.3553	0.495196	FALSE	-1.18803
xtr-miR-499_st	-42.3001	0.895983	FALSE	-1.18875	0.594799	FALSE	-40.7577
xtr-miR-7_st	-11.3513	0.298225	FALSE	-10.3364	0.698181	FALSE	-32.1635
xtr-miR-9_st	-34.8516	0.921093	FALSE	-19.8563	0.364252	FALSE	-31.3572
xtr-miR-92a_st	7.952853	2.05E-08	TRUE	8.248227	2.05E-08	TRUE	8.113422
xtr-miR-92b_st	3.481751	0.010726	TRUE	3.193766	0.070491	FALSE	2.591964
xtr-miR-93a_st	8.495754	2.05E-08	TRUE	8.20653	2.05E-08	TRUE	8.411358
xtr-miR-93b_st	8.241542	2.05E-08	TRUE	8.21855	2.05E-08	TRUE	8.0734
xtr-miR-96_st	-21.2465	0.355576	FALSE	-42.3897	0.788609	FALSE	-43.1851
xtr-miR-98_st	-41.989	0.885885	FALSE	-19.4567	0.315783	FALSE	-21.116
xtr-miR-99_st	-0.3619	0.187747	FALSE	-12.6066	0.489035	FALSE	1.706198
xtr-miR-9a_st	-43.1851	0.735295	FALSE	-43.1851	0.863303	FALSE	-42.8931
xtr-miR-9a-star_st	-42.8946	0.907665	FALSE	-42.8946	0.872518	FALSE	0.963104
xtr-miR-9b_st	-43.1851	0.825994	FALSE	-43.1851	0.86021	FALSE	-43.1851
xtr-miR-9b-star_st	0.787584	0.197249	FALSE	2.861818	0.058869	TRUE	1.455025
xtr-miR-9-star_st	-24.286	0.258701	FALSE	2.084072	0.380244	FALSE	-10.1243

p-value (Xt	Detection (	Xt lin28 MC	p-value (Xt	Detection (	Xt lin28 MC	p-value (Xt	Detection (	Xt lin28 MC
0.328373	FALSE	-21.4212	0.547572	FALSE	-25.0079	0.863629	FALSE	-36.6909
3.48E-06	TRUE	5.325869	3.17E-06	TRUE	5.981934	7.05E-06	TRUE	4.711016
2.05E-08	TRUE	8.560386	2.05E-08	TRUE	8.63938	2.05E-08	TRUE	8.497413
2.05E-08	TRUE	8.990183	2.05E-08	TRUE	9.269575	2.05E-08	TRUE	9.328463
2.05E-08	TRUE	10.63643	2.05E-08	TRUE	9.952602	2.05E-08	TRUE	10.64174
0.831764	FALSE	-26.8975	0.531331	FALSE	-27.3006	0.645205	FALSE	1.899738
0.30814	FALSE	3.435597	0.000962	TRUE	2.502017	0.106389	FALSE	0.499811
0.850283	FALSE	-30.1237	0.561021	FALSE	-20.639	0.592999	FALSE	-1.76254
0.209513	FALSE	1.800736	0.16769	FALSE	3.245998	0.062983	FALSE	1.902793
0.838556	FALSE	-21.2622	0.53214	FALSE	-20.869	0.274365	FALSE	-19.7956
0.946845	FALSE	-33.6423	0.686377	FALSE	-30.9551	0.444498	FALSE	-11.5458
0.736139	FALSE	-21.1506	0.528891	FALSE	-0.19292	0.492042	FALSE	-42.4781
0.93191	FALSE	-22.2701	0.502864	FALSE	-23.9069	0.699338	FALSE	-1.13729
0.832332	FALSE	1.553158	0.073101	FALSE	1.091898	0.300195	FALSE	-42.5366
0.17709	FALSE	-20.2132	0.261475	FALSE	-12.2806	0.456572	FALSE	-21.9914
0.948159	FALSE	2.008443	0.061553	FALSE	-0.15478	0.435013	FALSE	-1.70208
0.001288	TRUE	3.349402	0.00307	TRUE	4.288354	0.000149	TRUE	3.888323
2.05E-08	TRUE	9.121926	2.05E-08	TRUE	9.471471	2.05E-08	TRUE	9.165312
0.000375	TRUE	4.127491	0.004043	TRUE	5.084551	0.00013	TRUE	2.106804
0.350591	FALSE	-10.5436	0.57387	FALSE	-2.62314	0.64969	FALSE	-24.9428
0.811773	FALSE	-0.15678	0.205238	FALSE	-2.65255	0.126664	FALSE	2.328563
0.219691	FALSE	-43.1851	0.791248	FALSE	-3.69177	0.053514	TRUE	-43.1851
0.871332	FALSE	-20.8914	0.564966	FALSE	-20.8003	0.539009	FALSE	-20.5699
0.063582	FALSE	3.858928	0.001414	TRUE	2.791946	0.065729	FALSE	-42.5928
0.270017	FALSE	-21.142	0.427985	FALSE	-20.9626	0.614941	FALSE	-21.2263
0.507439	FALSE	0.36177	0.39859	FALSE	-42.1898	0.519455	FALSE	-43.1851
0.004859	TRUE	2.204479	0.005077	TRUE	-2.68847	0.674523	FALSE	1.993719
0.763466	FALSE	1.824518	0.069158	FALSE	-23.933	0.842256	FALSE	-21.8965
0.066446	FALSE	-19.4194	0.410638	FALSE	2.500037	0.016565	TRUE	3.450781
0.043286	TRUE	2.404584	0.038064	TRUE	2.426642	0.068236	FALSE	-42.3745
0.000428	TRUE	4.893084	1.63E-06	TRUE	4.524733	0.000252	TRUE	5.146558
2.46E-05	TRUE	6.619486	2.47E-07	TRUE	6.425005	2.86E-06	TRUE	6.269557
0.054425	TRUE	4.435192	2.29E-05	TRUE	3.176018	0.00865	TRUE	4.477327
0.72163	FALSE	-42.5895	0.964911	FALSE	-43.1851	0.899148	FALSE	-42.5895
0.617541	FALSE	-30.301	0.399301	FALSE	-43.0237	0.740408	FALSE	-1.76253
0.589419	FALSE	-19.4491	0.59438	FALSE	-25.9026	0.539218	FALSE	-43.1851
0.209703	FALSE	-20.8249	0.404649	FALSE	2.660362	0.138329	FALSE	0.630137
0.007354	TRUE	2.363935	0.118366	FALSE	2.414417	0.184038	FALSE	1.087999
0.834862	FALSE	-0.22391	0.240413	FALSE	1.504308	0.056994	TRUE	-43.1851
0.601771	FALSE	-0.1942	0.428257	FALSE	-0.06094	0.497555	FALSE	1.577738
0.895784	FALSE	-22.2735	0.558814	FALSE	-21.448	0.228819	FALSE	-42.9484
0.338246	FALSE	-35.2009	0.363599	FALSE	-9.673	0.28353	FALSE	-14.1398
0.01011	TRUE	0.401097	0.061516	FALSE	-20.4814	0.040408	TRUE	2.307837
0.545574	FALSE	-12.1932	0.33997	FALSE	-13.3306	0.375812	FALSE	-12.2126
0.243662	FALSE	0.846642	0.03496	TRUE	-4.681	0.184557	FALSE	0.336385
0.544721	FALSE	-21.1011	0.236867	FALSE	-20.7894	0.297999	FALSE	-22.171

0.347707	FALSE	-9.90939	0.32973	FALSE	-10.5521	0.353566	FALSE	-12.4839
0.125127	FALSE	1.647671	0.269629	FALSE	1.568013	0.321739	FALSE	2.602662
0.902191	FALSE	-7.94741	0.398816	FALSE	-8.61139	0.404103	FALSE	-6.47957
0.007074	TRUE	2.735069	0.020931	TRUE	1.597548	0.237567	FALSE	-20.1616
0.000387	TRUE	4.336757	1.52E-05	TRUE	2.025822	0.040513	TRUE	4.871256
0.164143	FALSE	2.992641	0.047162	TRUE	1.6884	0.112109	FALSE	-17.8241
0.116328	FALSE	1.163887	0.130743	FALSE	3.299948	0.028918	TRUE	0.668058
0.704192	FALSE	-18.7976	0.041759	TRUE	-21.1812	0.274434	FALSE	-19.8255
0.087803	FALSE	2.942271	0.023788	TRUE	-0.14855	0.495352	FALSE	-0.36307
0.022992	TRUE	3.174892	0.001967	TRUE	1.315225	0.233948	FALSE	-43.0888
9.37E-07	TRUE	4.004495	5.20E-05	TRUE	4.004702	0.000515	TRUE	4.989602
1.93E-05	TRUE	4.453246	1.44E-05	TRUE	4.398427	0.000167	TRUE	3.639747
0.068484	FALSE	4.064994	0.000188	TRUE	4.325184	2.68E-05	TRUE	3.362155
2.05E-08	TRUE	6.407911	5.08E-07	TRUE	7.256198	2.05E-08	TRUE	6.840498
2.05E-08	TRUE	7.368787	3.83E-08	TRUE	7.862497	2.47E-07	TRUE	7.824154
0.160653	FALSE	4.565835	0.000325	TRUE	3.663786	0.005198	TRUE	1.131627
2.05E-08	TRUE	7.921957	2.05E-08	TRUE	8.254768	2.05E-08	TRUE	7.923531
0.039277	TRUE	2.739011	0.034478	TRUE	-20.0116	0.218127	FALSE	2.834314
0.497952	FALSE	1.305795	0.401776	FALSE	-14.452	0.875527	FALSE	-24.2025
0.076736	FALSE	-19.9126	0.127285	FALSE	2.076237	0.070687	FALSE	-42.6095
0.000516	TRUE	3.984721	0.001771	TRUE	4.963558	0.000181	TRUE	5.354533
0.564609	FALSE	-31.4663	0.24981	FALSE	-32.0568	0.534717	FALSE	-31.4827
0.703855	FALSE	-0.10124	0.154927	FALSE	1.903227	0.116316	FALSE	-15.5578
0.769843	FALSE	3.20858	0.019788	TRUE	0.015331	0.308569	FALSE	-42.9462
0.403703	FALSE	3.196427	0.013097	TRUE	1.376184	0.369886	FALSE	-1.13
0.88736	FALSE	-1.24843	0.494706	FALSE	-0.81631	0.473265	FALSE	0.237922
0.561592	FALSE	-5.11659	0.041308	TRUE	-27.4035	0.4402	FALSE	-11.5472
2.05E-08	TRUE	7.100219	3.83E-08	TRUE	7.311665	2.47E-07	TRUE	7.019596
0.001224	TRUE	2.730502	0.017143	TRUE	4.872667	0.000188	TRUE	2.951081
2.86E-05	TRUE	5.610699	6.55E-07	TRUE	5.22169	3.72E-05	TRUE	4.862
0.00984	TRUE	-0.08318	0.27915	FALSE	-13.6505	0.745814	FALSE	2.416905
0.170318	FALSE	0.144538	0.117116	FALSE	-12.4128	0.788962	FALSE	1.577738
0.301918	FALSE	-21.109	0.700963	FALSE	-8.8469	0.367661	FALSE	2.392143
0.122199	FALSE	-8.64932	0.559329	FALSE	-7.82391	0.515288	FALSE	-7.07526
0.921775	FALSE	-0.26702	0.533555	FALSE	1.280213	0.397989	FALSE	0.298967
0.684778	FALSE	-35.6838	0.764882	FALSE	-34.6924	0.928144	FALSE	-34.2986
0.506399	FALSE	-34.9769	0.352301	FALSE	-19.8448	0.129735	FALSE	-34.9769
0.709278	FALSE	-14.2128	0.428089	FALSE	-10.6128	0.540687	FALSE	-11.1016
0.172386	FALSE	-14.4349	0.383789	FALSE	-9.97534	0.245079	FALSE	-25.2931
0.095752	FALSE	2.940126	0.003352	TRUE	2.192171	0.030683	TRUE	4.115733
2.05E-08	TRUE	8.739573	2.05E-08	TRUE	8.616715	2.05E-08	TRUE	8.847332
0.849052	FALSE	-43.1851	0.912687	FALSE	-20.4327	0.470694	FALSE	-42.5124
0.534777	FALSE	-43.1851	0.956198	FALSE	-43.1851	0.281027	FALSE	-17.713
0.728761	FALSE	-41.2029	0.240446	FALSE	-0.2387	0.251348	FALSE	-18.9591
0.237888	FALSE	2.896717	0.017736	TRUE	3.087454	0.037202	TRUE	1.559193
0.012575	TRUE	5.371216	1.47E-05	TRUE	2.878106	0.017926	TRUE	2.587478
0.832636	FALSE	2.351344	0.007626	TRUE	-30.0701	0.812432	FALSE	-8.28514

0.877165	FALSE	1.420871	0.195932	FALSE	-1.5594	0.396933	FALSE	1.926265
0.01288	TRUE	1.952091	0.068782	FALSE	-0.60187	0.146092	FALSE	3.478132
0.018209	TRUE	-21.2457	0.311488	FALSE	1.558136	0.160713	FALSE	3.752541
0.359951	FALSE	-22.3441	0.716837	FALSE	-22.3441	0.594686	FALSE	2.392145
0.120606	FALSE	2.293731	0.122924	FALSE	2.130812	0.080226	FALSE	3.248892
0.542304	FALSE	1.395218	0.040323	TRUE	-43.1851	0.862719	FALSE	-21.328
2.05E-08	TRUE	9.281268	2.05E-08	TRUE	9.381313	2.05E-08	TRUE	9.290119
0.892974	FALSE	1.834848	0.046284	TRUE	0.192639	0.290559	FALSE	-41.1117
2.05E-08	TRUE	9.031596	2.05E-08	TRUE	9.369553	2.05E-08	TRUE	9.056244
0.426202	FALSE	1.938599	0.057852	TRUE	0.113445	0.245397	FALSE	1.540994
0.152281	FALSE	-34.8363	0.765412	FALSE	-13.1221	0.548999	FALSE	-12.7632
1.04E-06	TRUE	7.189822	7.15E-08	TRUE	7.559833	1.33E-07	TRUE	7.888389
0.808867	FALSE	-27.16	0.526405	FALSE	-16.7305	0.680341	FALSE	2.482813
0.697531	FALSE	-21.0838	0.302396	FALSE	-22.5619	0.741451	FALSE	2.128872
0.269525	FALSE	-0.0407	0.182579	FALSE	-10.4197	0.365474	FALSE	-21.8967
0.066254	FALSE	-43.1851	0.104665	FALSE	-43.1851	0.056087	TRUE	-43.1851
0.485917	FALSE	-28.7115	0.614503	FALSE	-28.8347	0.539254	FALSE	-43.1851
1.30E-05	TRUE	5.730215	2.47E-07	TRUE	4.61208	0.000165	TRUE	5.650536
0.543053	FALSE	-43.1851	0.707593	FALSE	-22.0461	0.620663	FALSE	-21.661
0.245661	FALSE	5.346363	0.000259	TRUE	3.905141	0.006611	TRUE	4.457717
4.70E-05	TRUE	3.471024	0.000693	TRUE	3.196674	0.003146	TRUE	4.377936
0.792949	FALSE	2.269081	0.02651	TRUE	-42.8546	0.959966	FALSE	-1.03652
0.016077	TRUE	3.182415	0.009755	TRUE	-20.2648	0.512474	FALSE	1.499028
0.000802	TRUE	5.489844	1.73E-06	TRUE	5.394858	6.13E-05	TRUE	5.12585
2.38E-05	TRUE	5.782641	2.10E-06	TRUE	5.108821	0.000328	TRUE	6.261294
0.127472	FALSE	2.469342	0.074293	FALSE	2.141074	0.111175	FALSE	2.275885
0.444464	FALSE	-42.4901	0.815692	FALSE	-25.5006	0.394678	FALSE	-0.81097
0.000136	TRUE	3.863653	8.41E-06	TRUE	3.581337	0.000582	TRUE	5.375922
0.840055	FALSE	-0.05875	0.289666	FALSE	-43.1851	0.928627	FALSE	-42.2859
0.028163	TRUE	-41.4771	0.693315	FALSE	0.387725	0.058115	TRUE	-41.4771
0.729746	FALSE	-43.1851	0.99739	FALSE	-43.1851	0.975272	FALSE	-43.1851
0.75827	FALSE	-43.1714	0.792494	FALSE	1.571674	0.277169	FALSE	-43.1714
0.82765	FALSE	-43.1851	0.979216	FALSE	-23.933	0.845334	FALSE	-21.3393
0.881274	FALSE	-32.2584	0.804585	FALSE	1.55805	0.350928	FALSE	-10.1335
0.943128	FALSE	-36.2972	0.548129	FALSE	-20.2408	0.77625	FALSE	-43.1851
0.905996	FALSE	-43.1851	0.338165	FALSE	-12.2134	0.188262	FALSE	-43.1851
0.254528	FALSE	0.585006	0.40611	FALSE	0.20643	0.234764	FALSE	0.859524
0.487732	FALSE	-43.1851	0.809428	FALSE	0.530593	0.251348	FALSE	-1.18178
0.942468	FALSE	-15.9179	0.471975	FALSE	-16.3905	0.74374	FALSE	-17.296
0.220877	FALSE	2.526856	0.007359	TRUE	-2.21883	0.16008	FALSE	3.701097
7.15E-08	TRUE	5.757265	1.04E-06	TRUE	5.250952	1.79E-06	TRUE	5.201756
5.81E-06	TRUE	5.454705	2.46E-06	TRUE	5.288107	5.00E-05	TRUE	6.226299
0.000473	TRUE	4.026482	0.008247	TRUE	5.971286	9.25E-06	TRUE	4.126297
0.054325	TRUE	2.646142	0.016151	TRUE	3.541151	0.002406	TRUE	1.916482
0.621482	FALSE	-13.3809	0.255887	FALSE	-33.2935	0.419208	FALSE	-36.5567
0.25967	FALSE	3.118572	0.008506	TRUE	-20.1228	0.380171	FALSE	-19.6011
0.404946	FALSE	-19.573	0.122343	FALSE	2.324159	0.097806	FALSE	-0.19981

0.973645	FALSE	-43.1851	0.704368	FALSE	-43.1851	0.976958	FALSE	-20.9111
0.489571	FALSE	-0.02839	0.487195	FALSE	-0.54239	0.131228	FALSE	-13.0882
0.440387	FALSE	-13.8854	0.174592	FALSE	-22.2868	0.575308	FALSE	-14.1478
0.415497	FALSE	-23.2437	0.241689	FALSE	1.776679	0.244679	FALSE	-15.5864
0.52411	FALSE	-43.1851	0.868019	FALSE	-14.1866	0.717095	FALSE	-43.1851
3.83E-08	TRUE	6.148001	1.04E-06	TRUE	6.34268	1.18E-07	TRUE	6.503258
2.05E-08	TRUE	5.989089	2.10E-06	TRUE	6.974486	4.57E-07	TRUE	6.330425
0.055748	TRUE	-0.96011	0.182781	FALSE	1.222319	0.091566	FALSE	2.60076
0.029263	TRUE	1.470863	0.005341	TRUE	1.088065	0.154136	FALSE	-15.1301
0.629233	FALSE	-33.1551	0.532293	FALSE	-33.1551	0.919417	FALSE	-22.4738
0.619779	FALSE	1.281147	0.203737	FALSE	-26.7613	0.860672	FALSE	-0.38894
0.512961	FALSE	-21.2962	0.269445	FALSE	-21.543	0.440082	FALSE	1.733786
2.05E-08	TRUE	11.13727	2.05E-08	TRUE	10.46557	2.05E-08	TRUE	11.07737
0.442603	FALSE	-43.1851	0.985758	FALSE	-14.0679	0.574754	FALSE	-20.9111
0.082731	FALSE	2.366652	0.00448	TRUE	2.874937	0.061483	FALSE	1.778406
0.471402	FALSE	-10.351	0.271474	FALSE	-29.4618	0.769322	FALSE	-18.8675
0.102572	FALSE	1.73073	0.005718	TRUE	2.697119	0.128943	FALSE	2.598151
0.105122	FALSE	0.980881	0.328871	FALSE	-21.0082	0.735795	FALSE	-21.328
0.628912	FALSE	-32.7856	0.202949	FALSE	-41.9854	0.929163	FALSE	-41.9854
0.763466	FALSE	-42.1711	0.744347	FALSE	-23.6838	0.693507	FALSE	-40.7859
0.926601	FALSE	-10.4374	0.60076	FALSE	-9.74129	0.470871	FALSE	-11.4522
0.705053	FALSE	-34.8516	0.77754	FALSE	-18.6147	0.494679	FALSE	-20.4341
2.05E-08	TRUE	7.91367	2.05E-08	TRUE	8.079785	2.05E-08	TRUE	8.315454
0.183327	FALSE	3.861247	0.004135	TRUE	3.453926	0.024406	TRUE	-19.6617
2.05E-08	TRUE	8.460296	2.05E-08	TRUE	8.416346	2.05E-08	TRUE	8.520145
2.05E-08	TRUE	8.444076	2.05E-08	TRUE	8.479532	2.05E-08	TRUE	8.190845
0.934019	FALSE	1.986729	0.010169	TRUE	-42.3897	0.903614	FALSE	-42.3897
0.630148	FALSE	-20.4336	0.591195	FALSE	-43.1851	0.961463	FALSE	0.94598
0.51266	FALSE	0.017668	0.372904	FALSE	-1.71053	0.436666	FALSE	-13.4037
0.491375	FALSE	-43.1851	0.854651	FALSE	-42.4561	0.554033	FALSE	-43.1851
0.517578	FALSE	1.15408	0.049764	TRUE	0.09424	0.267403	FALSE	-1.9523
0.571661	FALSE	-30.1074	0.498304	FALSE	-28.4756	0.597349	FALSE	-43.1851
0.227638	FALSE	1.957795	0.06162	FALSE	3.311613	0.017741	TRUE	-19.4844
0.234045	FALSE	-24.7435	0.15142	FALSE	-28.4405	0.646671	FALSE	-3.29303

p-value (Xt	Detection (Xt lin28 MO s10.5_3.CEL)
0.255675	FALSE
0.000422	TRUE
2.05E-08	TRUE
2.05E-08	TRUE
2.05E-08	TRUE
0.463603	FALSE
0.393362	FALSE
0.335471	FALSE
0.213904	FALSE
0.218795	FALSE
0.548227	FALSE
0.604195	FALSE
0.608819	FALSE
0.81228	FALSE
0.318829	FALSE
0.365848	FALSE
0.002576	TRUE
2.05E-08	TRUE
0.023572	TRUE
0.836384	FALSE
0.052098	TRUE
0.982889	FALSE
0.403722	FALSE
0.48414	FALSE
0.357256	FALSE
0.83286	FALSE
0.057481	TRUE
0.765292	FALSE
0.009729	TRUE
0.776921	FALSE
9.67E-06	TRUE
1.34E-06	TRUE
0.000159	TRUE
0.893252	FALSE
0.330951	FALSE
0.989468	FALSE
0.397341	FALSE
0.132221	FALSE
0.940649	FALSE
0.227786	FALSE
0.7899	FALSE
0.554332	FALSE
0.003154	TRUE
0.332443	FALSE
0.052297	TRUE
0.696646	FALSE

0.759887	FALSE
0.096458	FALSE
0.438821	FALSE
0.10893	FALSE
0.000306	TRUE
0.051993	TRUE
0.271188	FALSE
0.207697	FALSE
0.030176	TRUE
0.305566	FALSE
4.52E-06	TRUE
0.001576	TRUE
0.005443	TRUE
2.05E-08	TRUE
2.05E-08	TRUE
0.191083	FALSE
2.05E-08	TRUE
0.044551	TRUE
0.968696	FALSE
0.608284	FALSE
0.000705	TRUE
0.395173	FALSE
0.600559	FALSE
0.639357	FALSE
0.128741	FALSE
0.162074	FALSE
0.081363	FALSE
3.83E-08	TRUE
0.042148	TRUE
0.00015	TRUE
0.100272	FALSE
0.160703	FALSE
0.469001	FALSE
0.310543	FALSE
0.366011	FALSE
0.726427	FALSE
0.535276	FALSE
0.373213	FALSE
0.970546	FALSE
0.000651	TRUE
2.05E-08	TRUE
0.547122	FALSE
0.490709	FALSE
0.264433	FALSE
0.347051	FALSE
0.010038	TRUE
0.334032	FALSE

0.152103	FALSE
0.01162	TRUE
0.002483	TRUE
0.125555	FALSE
0.03992	TRUE
0.742255	FALSE
2.05E-08	TRUE
0.942076	FALSE
2.05E-08	TRUE
0.2044	FALSE
0.520162	FALSE
2.05E-08	TRUE
0.180145	FALSE
0.374537	FALSE
0.835802	FALSE
0.094049	FALSE
0.916107	FALSE
6.37E-06	TRUE
0.580769	FALSE
0.006778	TRUE
1.72E-05	TRUE
0.392168	FALSE
0.083914	FALSE
4.13E-05	TRUE
5.08E-07	TRUE
0.088147	FALSE
0.095861	FALSE
5.08E-07	TRUE
0.90082	FALSE
0.48669	FALSE
0.90951	FALSE
0.462409	FALSE
0.671552	FALSE
0.65773	FALSE
0.944119	FALSE
0.946499	FALSE
0.367331	FALSE
0.532092	FALSE
0.734397	FALSE
0.043361	TRUE
1.21E-06	TRUE
1.34E-06	TRUE
0.00252	TRUE
0.023026	TRUE
0.765679	FALSE
0.080219	FALSE
0.369764	FALSE

0.579915	FALSE
0.602517	FALSE
0.197498	FALSE
0.202911	FALSE
0.964548	FALSE
3.83E-08	TRUE
4.06E-07	TRUE
0.03912	TRUE
0.89015	FALSE
0.78965	FALSE
0.156661	FALSE
0.101719	FALSE
2.05E-08	TRUE
0.50218	FALSE
0.034363	TRUE
0.505389	FALSE
0.06391	FALSE
0.593493	FALSE
0.685152	FALSE
0.447483	FALSE
0.649829	FALSE
0.540126	FALSE
2.05E-08	TRUE
0.171753	FALSE
2.05E-08	TRUE
2.05E-08	TRUE
0.849027	FALSE
0.145711	FALSE
0.790316	FALSE
0.741247	FALSE
0.604478	FALSE
0.914759	FALSE
0.033151	TRUE
0.363439	FALSE

		LogMedianRatios				
		282 CoMo	282 A+B	285 CoMo	285 a+B M	284 CoMO
Probe Id	Annotation	Slide 1	Slide 2	Slide 3	Slide 4	Slide 5
50272	xtr-miR-20a	0.49	-1.66	0.77	-0.39	0.48
46777	xtr-miR-17-5p	0.30	-1.29	0.45	-0.58	0.24
10998	xtr-miR-19b	0.27	-1.20	0.70	-0.21	-0.02
11000	xtr-miR-200a	0.28	-1.15	0.58	-0.31	0.06
13143	xtr-miR-301	0.21	-1.22	0.53	-0.53	-0.29
18900	xtr-miR-200b	0.37	-1.03	0.76	0.05	0.17
48946	xtr-miR-428	-0.22	-1.59	0.77	0.09	0.32
10997	xtr-miR-19a	0.27	-1.05	0.88	-0.14	0.06
42860	xtr-miR-20b	0.18	-1.13	0.61	-0.31	0.28
11077	xtr-miR-363-3p	0.24	-0.95	0.60	-0.44	0.20
29490	xtr-miR-7	-0.22	0.79	0.25	-0.26	-0.41
49301	xtr-miR-203	0.06	-0.92	0.53	-0.04	-0.09
10936	xtr-miR-130b	0.35	-0.49	0.49	-0.06	0.35
17565	xtr-miR-30b	0.08	-0.39	0.08	0.01	0.36
11020	xtr-miR-22	-0.19	-0.41	0.11	0.50	-0.30
48927	xtr-miR-125a	0.26	0.15	0.55	0.23	0.19
4610	xtr-miR-126	1.10	1.11	1.40	1.11	1.38
10964	xtr-miR-155	-0.17	0.03	0.09	0.30	0.41
19004	xtr-let-7c	0.12	0.17	0.15	0.24	0.16
50002	xtr-miR-427	0.03	0.05	-0.12	-0.15	0.41
49680	xtr-let-7e	-0.21	-0.26	0.13	0.13	-0.09
17748	xtr-let-7a	0.16	0.05	0.14	0.22	0.34
42588	xtr-miR-18a	-0.04	-1.24	0.46	-0.57	NA
13141	xtr-miR-18b	0.22	-1.10	0.71	-0.40	NA
49406	xtr-miR-130c	-0.01	-1.09	0.44	-0.45	NA
42923	xtr-miR-30c	0.02	-0.17	-0.24	-0.28	NA
49599	xtr-miR-367	0.01	-0.55	0.44	0.15	NA
17478	xtr-miR-429	0.37	-0.78	0.29	-0.22	NA
42467	xtr-miR-129	0.46	0.68	NA	0.26	NA
42532	xtr-miR-22*	-0.13	NA	0.33	0.17	NA
27217	xtr-miR-34a	-0.30	0.07	NA	0.26	NA
30687	xtr-miR-93a	0.21	-0.14	0.29	NA	NA
30755	xtr-miR-133b	0.61	NA	0.58	NA	NA
42802	xtr-miR-150	NA	0.20	NA	NA	NA
27544	xtr-miR-363-5p	NA	-0.12	0.15	NA	NA
14328	xtr-miR-124	NA	NA	0.66	NA	NA
10947	xtr-miR-142-3p	NA	0.57	NA	NA	NA
11007	xtr-miR-206	NA	NA	0.62	NA	NA
42744	xtr-miR-23a	NA	-0.22	NA	NA	NA
11030	xtr-miR-26	NA	-0.64	NA	NA	NA
49610	xtr-miR-302	NA	0.34	NA	NA	NA
28191	xtr-miR-30e	NA	NA	0.24	NA	NA
11074	xtr-miR-34b	NA	NA	0.47	NA	NA
49640	xtr-miR-449	NA	NA	0.57	NA	NA

49532	xtr-let-7b	NA	NA	NA	NA	NA
17752	xtr-let-7f	NA	NA	NA	NA	NA
50237	xtr-let-7g	NA	NA	NA	NA	NA
19580	xtr-let-7i	NA	NA	NA	NA	NA
19581	xtr-miR-100	NA	NA	NA	NA	NA
31026	xtr-miR-101a	NA	NA	NA	NA	NA
10919	xtr-miR-103	NA	NA	NA	NA	NA
46629	xtr-miR-107	NA	NA	NA	NA	NA
13485	xtr-miR-10a	NA	NA	NA	NA	NA
10925	xtr-miR-10b	NA	NA	NA	NA	NA
49570	xtr-miR-10c	NA	NA	NA	NA	NA
19583	xtr-miR-122	NA	NA	NA	NA	NA
30787	xtr-miR-125b	NA	NA	NA	NA	NA
33596	xtr-miR-126*	NA	NA	NA	NA	NA
33902	xtr-miR-128	NA	NA	NA	NA	NA
10138	xtr-miR-130a	NA	NA	NA	NA	NA
10937	xtr-miR-132	NA	NA	NA	NA	NA
49449	xtr-miR-133a	NA	NA	NA	NA	NA
49086	xtr-miR-133c	NA	NA	NA	NA	NA
49925	xtr-miR-133d	NA	NA	NA	NA	NA
42839	xtr-miR-135	NA	NA	NA	NA	NA
10944	xtr-miR-137	NA	NA	NA	NA	NA
13140	xtr-miR-138	NA	NA	NA	NA	NA
49072	xtr-miR-139	NA	NA	NA	NA	NA
4700	xtr-miR-140	NA	NA	NA	NA	NA
19015	xtr-miR-142-5p	NA	NA	NA	NA	NA
13177	xtr-miR-143	NA	NA	NA	NA	NA
29802	xtr-miR-144	NA	NA	NA	NA	NA
42641	xtr-miR-145	NA	NA	NA	NA	NA
49521	xtr-miR-146	NA	NA	NA	NA	NA
49833	xtr-miR-146b	NA	NA	NA	NA	NA
10955	xtr-miR-148a	NA	NA	NA	NA	NA
19585	xtr-miR-148b	NA	NA	NA	NA	NA
42599	xtr-miR-153	NA	NA	NA	NA	NA
27720	xtr-miR-15a	NA	NA	NA	NA	NA
49276	xtr-miR-15b	NA	NA	NA	NA	NA
17280	xtr-miR-15c	NA	NA	NA	NA	NA
48930	xtr-miR-16a	NA	NA	NA	NA	NA
49776	xtr-miR-16b	NA	NA	NA	NA	NA
50387	xtr-miR-16c	NA	NA	NA	NA	NA
19588	xtr-miR-17-3p	NA	NA	NA	NA	NA
42865	xtr-miR-181a	NA	NA	NA	NA	NA
49938	xtr-miR-181a-1*	NA	NA	NA	NA	NA
50086	xtr-miR-181a-2*	NA	NA	NA	NA	NA
30121	xtr-miR-181b	NA	NA	NA	NA	NA
10975	xtr-miR-182	NA	NA	NA	NA	NA
10976	xtr-miR-182*	NA	NA	NA	NA	NA

10977	xtr-miR-183	NA	NA	NA	NA	NA
10978	xtr-miR-184	NA	NA	NA	NA	NA
49906	xtr-miR-189	NA	NA	NA	NA	NA
13178	xtr-miR-18a*	NA	NA	NA	NA	NA
10985	xtr-miR-191	NA	NA	NA	NA	NA
48914	xtr-miR-193	NA	NA	NA	NA	NA
10988	xtr-miR-194	NA	NA	NA	NA	NA
10990	xtr-miR-196a	NA	NA	NA	NA	NA
49827	xtr-miR-196b	NA	NA	NA	NA	NA
29562	xtr-miR-199a	NA	NA	NA	NA	NA
10995	xtr-miR-199a*	NA	NA	NA	NA	NA
48926	xtr-miR-199b	NA	NA	NA	NA	NA
10916	xtr-miR-1a	NA	NA	NA	NA	NA
49485	xtr-miR-1b	NA	NA	NA	NA	NA
50392	xtr-miR-202	NA	NA	NA	NA	NA
49322	xtr-miR-202*	NA	NA	NA	NA	NA
11005	xtr-miR-204	NA	NA	NA	NA	NA
42655	xtr-miR-205a	NA	NA	NA	NA	NA
49907	xtr-miR-205b	NA	NA	NA	NA	NA
49565	xtr-miR-208	NA	NA	NA	NA	NA
50350	xtr-miR-20a*	NA	NA	NA	NA	NA
42797	xtr-miR-210	NA	NA	NA	NA	NA
50000	xtr-miR-212	NA	NA	NA	NA	NA
11014	xtr-miR-214	NA	NA	NA	NA	NA
42553	xtr-miR-216	NA	NA	NA	NA	NA
19016	xtr-miR-217	NA	NA	NA	NA	NA
11018	xtr-miR-218	NA	NA	NA	NA	NA
42509	xtr-miR-219	NA	NA	NA	NA	NA
11022	xtr-miR-221	NA	NA	NA	NA	NA
11023	xtr-miR-222	NA	NA	NA	NA	NA
11024	xtr-miR-223	NA	NA	NA	NA	NA
46721	xtr-miR-23b	NA	NA	NA	NA	NA
28376	xtr-miR-24a	NA	NA	NA	NA	NA
49259	xtr-miR-24b	NA	NA	NA	NA	NA
42682	xtr-miR-25	NA	NA	NA	NA	NA
46483	xtr-miR-27a	NA	NA	NA	NA	NA
46469	xtr-miR-27b	NA	NA	NA	NA	NA
49209	xtr-miR-27c	NA	NA	NA	NA	NA
49292	xtr-miR-29a	NA	NA	NA	NA	NA
11041	xtr-miR-29a/xtr-miR-29c	NA	NA	NA	NA	NA
11040	xtr-miR-29b	NA	NA	NA	NA	NA
49438	xtr-miR-29c*	NA	NA	NA	NA	NA
49495	xtr-miR-29d	NA	NA	NA	NA	NA
50243	xtr-miR-30a-3p	NA	NA	NA	NA	NA
50388	xtr-miR-30a-5p	NA	NA	NA	NA	NA
19596	xtr-miR-30d	NA	NA	NA	NA	NA
49344	xtr-miR-31	NA	NA	NA	NA	NA

50014	xtr-miR-31b	NA	NA	NA	NA	NA
49606	xtr-miR-320	NA	NA	NA	NA	NA
42592	xtr-miR-338	NA	NA	NA	NA	NA
11062	xtr-miR-33a	NA	NA	NA	NA	NA
49314	xtr-miR-33b	NA	NA	NA	NA	NA
11078	xtr-miR-365	NA	NA	NA	NA	NA
42498	xtr-miR-375	NA	NA	NA	NA	NA
11098	xtr-miR-383	NA	NA	NA	NA	NA
17608	xtr-miR-425-5p	NA	NA	NA	NA	NA
42866	xtr-miR-451	NA	NA	NA	NA	NA
49412	xtr-miR-455	NA	NA	NA	NA	NA
49630	xtr-miR-489	NA	NA	NA	NA	NA
14313	xtr-miR-499	NA	NA	NA	NA	NA
11185	xtr-miR-9*/xtr-miR-9a*	NA	NA	NA	NA	NA
7190	xtr-miR-9/xtr-miR-9a	NA	NA	NA	NA	NA
42728	xtr-miR-92a	NA	NA	NA	NA	NA
17718	xtr-miR-92b	NA	NA	NA	NA	NA
50271	xtr-miR-93a/xtr-miR-93b	NA	NA	NA	NA	NA
13147	xtr-miR-96	NA	NA	NA	NA	NA
11182	xtr-miR-98	NA	NA	NA	NA	NA
42708	xtr-miR-99	NA	NA	NA	NA	NA
4040	xtr-miR-9a	NA	NA	NA	NA	NA
50168	xtr-miR-9b	NA	NA	NA	NA	NA
50215	xtr-miR-9b*	NA	NA	NA	NA	NA

284 A+B

Slide 6	count
-1.12	6
-1.01	6
-0.76	6
-0.96	6
-0.98	6
-0.73	6
-0.99	6
-0.67	6
-0.82	6
-0.84	6
0.34	6
-0.41	6
-0.14	6
-0.12	6
-0.23	6
0.06	6
1.57	6
0.27	6
0.35	6
0.24	6
0.05	6
0.27	6
-1.02	
-0.63	
NA	
NA	
NA	
NA	
NA	
NA	
NA	
NA	
NA	
0.64	
NA	
NA	
NA	
NA	
NA	
NA	
NA	
NA	
NA	
NA	

NA
NA
NA
NA
NA
NA
NA
NA
NA
NA
NA
NA
NA
NA
NA
NA
NA
NA
NA
NA
NA
NA
NA
NA
NA
NA
NA
NA
NA
NA
NA
NA
NA
NA
NA
NA
NA
NA
NA
NA
NA
NA
NA
NA
NA
NA
NA

NA
NA
NA
NA
NA
NA
NA
NA
NA
NA
NA
NA
NA
NA
NA
NA
NA
NA
NA
NA
NA
NA
NA
NA
NA
NA
NA
NA
NA
NA
NA
NA
NA
NA
NA
NA
NA
NA
NA
NA
NA
NA
NA
NA
NA
NA
NA

NA
NA
NA
NA
NA
NA
NA
NA
NA
NA
NA
NA
NA
NA
NA
NA
NA
NA
NA
NA
NA
NA
NA
NA
NA